Bio-Design and Manufacturing (2025) 8:877–908
https://doi.org/10.1631/bdm.2400363

REVIEW

Complexities and challenges associated with articular cartilage tissue defect reconstruction: an overview of bioprinting therapeutics

Parichita Mishra[1] · Vidhi Manish Badiyani[1] · Abhishek Kumar Singh[2] · Vivek Pandey[3] · Manash Kumar Paul[4] · Kanive Parashiva Guruprasad[5] · Bhisham Narayan Singh[1]

Received: 9 September 2024 / Accepted: 12 February 2025

Abstract

Osteoarthritis is a common aging-related disorder that is confined mostly to the chondral layer of joints (e.g., the knee) but can spread to bony layers over time. In its early stages, osteoarthritis has minimal symptoms; however, these gradually worsen over time and include joint pain, stiffness, loss of mobility, and inflammation. The exposed subchondral bone of a Grade 4 osteoarthritic knee is highly prone to erosion if left untreated due to persistent rubbing between the bones, which can lead to painful bone spurs. However, treating osteoarthritis is especially challenging due to the poor mitotic potential and low metabolic activity of chondrocytes. Although currently available tissue-engineered products (e.g., BST-CarGel®, TruFit®, and Atelocollagen®) can achieve structural reconstruction and tissue regeneration, final clinical outcomes can still be improved. Major challenges faced during clinical studies of tissue-engineered constructs include chondrocyte hypertrophy and the development of mechanically inferior fibrous tissue, among others. These issues can be addressed by selecting suitable biomaterial combinations, mimicking the three-dimensional (3D) architecture of the tissue matrix, and better controlling inflammation. Furthermore, it is crucial to generate essential signaling molecules within the articular cartilage ecosystem. This approach must also account for the microarchitecture of the affected joint and support the chondrogenic differentiation of mesenchymal stem cells. The use of tissue-engineered constructs has the potential to overcome each of these challenges, since materials can be modified for drug/biomolecule delivery while simultaneously facilitating the regeneration of robust articular cartilage. Three-dimensional printing has been successfully used in tissue engineering to achieve bioprinting. By manipulating conventional 3D printing techniques and the types of bioink used, many different types of bioprinting have emerged. Overall, these bioprinting techniques can be used to address various challenges associated with osteoarthritis treatment.

✉ Bhisham Narayan Singh
bhisham.singh@manipal.edu

[1] Department of Biotechnology, Manipal School of Life Sciences, Manipal Academy of Higher Education, Manipal 576104, India

[2] Manipal Centre for Biotherapeutics Research, Manipal Academy of Higher Education, Manipal 576104, India

[3] Department of Orthopaedics, Kasturba Medical College, Manipal Academy of Higher Education, Manipal 576104, India

[4] Department of Radiation Biology and Toxicology, Manipal School of Life Sciences, Manipal Academy of Higher Education, Manipal 576104, India

[5] Department of Ageing Research, Manipal School of Life Sciences, Manipal Academy of Higher Education, Manipal 576104, India

Graphical abstract

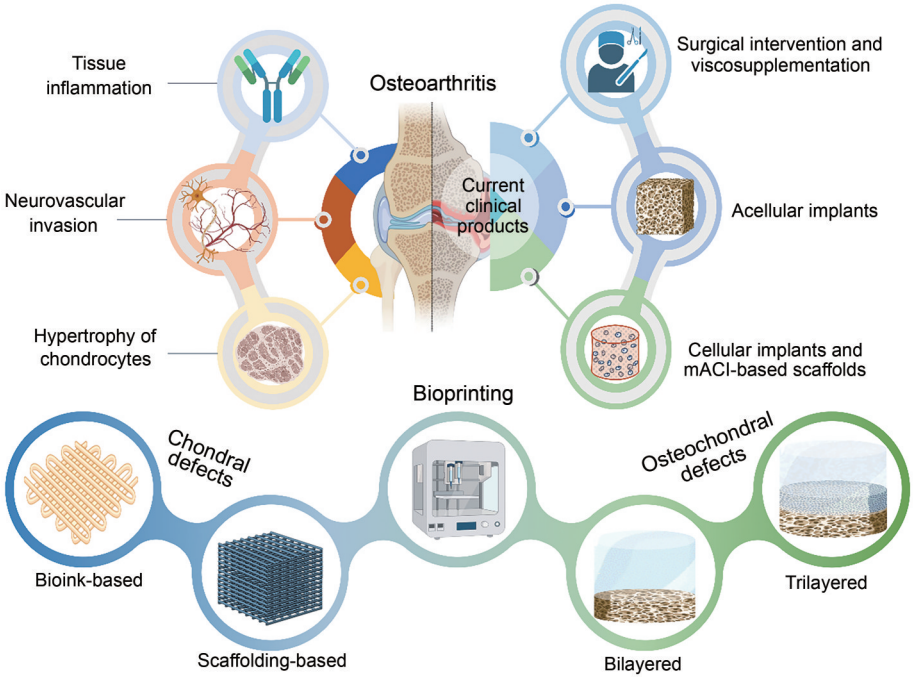

Keywords Articular cartilage · Biomaterials · Bioprinting · Osteoarthritis · Tissue engineering

1 Introduction

Articular cartilage is a type of specialized connective tissue required for maintaining the skeletal frame, and its systematic positioning facilitates its functionality [1]. It comprises a unique composition of extracellular matrix (ECM) components responsible for load-bearing properties [1, 2]. The articular cartilage ECM is mainly composed of water (80%), with the remainder being molecules such as proteoglycans and collagen [3]. These ECM components help joints absorb shock and resist wear and tear [2]. Overall, articular cartilage is an avascular and aneural tissue, with the total chondrocyte population comprising only 2% of total tissue volume [2]. This population consists of mature cells that are responsible for ECM remodeling; moreover, they do not possess a proliferative phenotype in adults [4], with proliferative cartilage progenitor cells (CPCs) found only during the developmental and growth stages [5]. Cartilage growth generally begins in the early twenties and is usually characterized by complete ossification of the epiphyseal plate [5, 6]. This also isolates mature articular cartilage tissue from bone marrow, which is the main source of mesenchymal stem cells (MSCs), the progenitors of CPCs [6]. This isolation causes articular cartilage to have poor mitotic potential and poor regenerative ability [1, 6]. Moreover, since joints with articular cartilage are highly active, loss of cartilage is often accompanied by continual loss of articular cartilage tissue over time, an effect that can lead to cartilage degeneration disorders such as osteoarthritis. Osteoarthritis is a common age-associated disorder, affecting more than 88% of the population over the age of 45 [7]. Osteoarthritis incidence is also associated with comorbidities such as diabetes, obesity, improper loading of joints, and injuries. Furthermore, osteoarthritis is more prevalent in women, who comprise 62% of the total affected population [7]. Globally, 242 million people are thought to be regularly affected by knee and/or hip osteoarthritis alone [8], with the prevalence of osteoarthritis increasing by 113.25% over the past several decades, from 247.51 million in 1990 to 527.81 million in 2019 [9].

The inability of articular cartilage to regenerate naturally and efficiently is a challenge for treating osteoarthritis. Current clinical strategies can be broadly classified into surgical and non-surgical approaches [10]. Non-surgical approaches include supplements such as glucosamine, hyaluronic acid, and steroids, as well as activities such as physiotherapy [10]. Such treatments may alleviate symptoms and improve joint function in some patients; however, they do not provide a permanent solution and require continuous administration to maintain positive effects. Furthermore, clinical studies have shown that some supplements—e.g., glucosamine and

chondroitin sulfate—are not totally effective when administered to reduce pain and inflammation in osteoarthritis patients, often yielding limited improvement relative to a placebo [11]. Steroid injections, though effective in providing short-term relief, may also result in potential adverse effects with repeated use, including joint tissue damage and accelerated cartilage degradation [12]. Non-surgical treatments thus have notable limitations with respect to providing long-term relief or halting disease progression, since they focus primarily on symptom management rather than cartilage regeneration or joint repair. Surgical approaches include procedures such as microfractures, abrasion chondroplasty, and arthroplasty, among others [10]. Surgical procedures such as microfractures often result in the formation of fibrous scar tissue, which can result in joint stiffness and pain. This can lead to recurring osteoarthritis due to the wear and tear of mechanically inferior regenerated tissue [8]. Thus, novel treatments designed to overcome the drawbacks of traditional treatment modalities—including those involving advances in tissue engineering and regenerative medicine—have been highly sought after. This is evident from the increasing number of publications in the field of cartilage regeneration, as shown in Fig. 1.

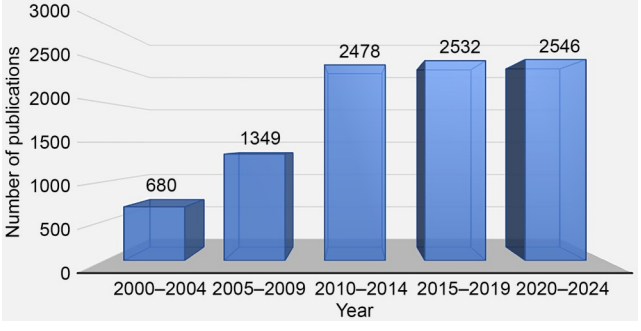

Fig. 1 Scientific publications (i.e., books, clinical trials, research studies, and review manuscripts) that have been published within the last 25 years. Data were taken from PubMed®, checked on 25th November, 2024, using the keyword "cartilage regeneration." These data suggest increasing interest in this field of research

Tissue engineering is an interdisciplinary field that integrates the use of biomaterials and biomolecules to aid the regeneration of various affected tissues. Cartilage tissue engineering aims to target the inherent tendency for tissue hypertrophy while maintaining the superior biomechanical characteristics of engineered tissue. Many tissue-engineered products, including ChonDux™, EUFLEXXA®, and HYMOVIS®, have been developed to treat osteoarthritis. These products employ various biocompatible biomaterials such as chondroitin sulfate, hyaluronic acid, and poly(ethylene glycol), all of which are used to form hydrogels that can not only support the growth of chondrocytes but also mimic the native ECM. Furthermore, tissue-engineered products such as NeoCart® have been incorporated into surgical procedures such as autologous chondrocyte implantation (ACI) to improve the regeneration of articular cartilage.

ACI is a procedure in which autologous chondrocytes (harvested from the patient beforehand) are cultured in vitro before being implanted at the defect site. The first two generations of ACI use a periosteal patch (also harvested from the patient) or a collagen patch to cover the site where autologous chondrocytes are injected [9]. The third generation involves the rise of matrix-assisted ACI (mACI), in which collagen-based scaffolds such as Hyalograft® C are incorporated with autologous chondrocytes [9]. The fourth generation of ACI features exploration of various biomaterials and cell types along with the addition of growth factors [9]. However, during delamination in ACI treatment, cartilage and fibrocartilage differentiations are similar. To date, no previous study has been able to mimic the intricate microarchitecture of various zones of articular cartilage. Newer tissue engineering strategies such as bioprinting have been successful in addressing this issue, since they depend on a layer-by-layer approach. This permits the design of accurate tissue analogs using different types of cells, biomaterials, and essential biomolecules.

2 The articular cartilage ecosystem and osteoarthritis pathophysiology

Articular cartilage is a highly mechanosensitive tissue that has a range of time-dependent and time-independent behaviors that can be non-linear or anisotropic [3]. Native articular cartilage has a tensile Young's modulus of 5–25 MPa, a compressive Young's modulus of 0.24–0.85 MPa, a tensile strength of 15–35 MPa, and a compressive strength of 14–59 MPa [3, 10]. Mature articular cartilage comprises chondrocytes, which are differentiated cells that maintain the articular cartilage ECM [1]. In general, ECM molecules and chondrocytes maintain the delicate tissue microenvironment and ensure efficient diarthrodial joint functioning, as listed in Table S1 (supplementary information). Chondrocytes themselves are bound to the ECM via integrins, decorins, perlecan, and collagen type 6. These molecules then form larger networks with aggrecan, collagen type 2, hyaluronic acid (assisted by collagen types 9 and 11 and link proteins), matrilin, and cartilage oligomeric matrix proteins (COMPs) [3]. This combination forms a chondron that comprises eight chondrocytes. Furthermore, the arrangement of chondrons determines the unique hierarchical organization within the articular cartilage tissue, which can then be categorized into four distinct zones, as shown in Fig. 2.

Zone 1, also known as the superficial zone, comprises the anterior face of the tissue and is in direct contact with the articular surface. Here, chondrocytes are embedded in

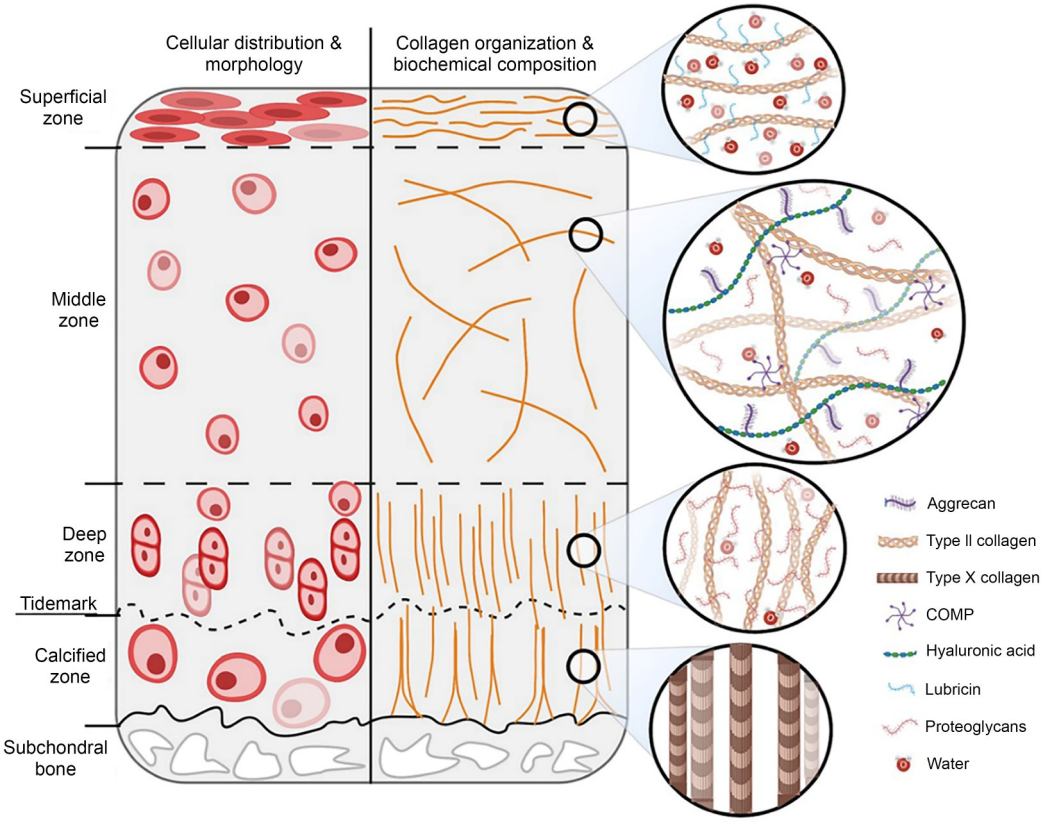

Fig. 2 Chondrocyte zonal distribution in articular cartilage along with collagen fibrils. This combination is essential in facilitating the load-bearing properties of the joint. The functions of the various ECM components are listed in Table S1 (supplementary information). Reproduced from [26], Copyright 2021, with permission from the authors, licensed under CC BY 4.0

compactly packed collagen type 2 fibers with diameters ranging from 15 to 25 nm that are organized tangentially to the articular surface [1, 13]. The chondrocytes in Zone 1 are present in high numbers but are generally inactive and have a flatter morphology than those in the middle zone [3]. The superficial zone protects other layers from shear stresses and regulates the flow of joint fluids during compression [2]. Zone 2, also known as the middle zone, also bears the initial brunt of any compressive loads applied to diarthrodial joints [3]. Collagen type 2 fibers are relatively thick, with diameters ranging from 40 to 100 nm, and they are arranged at random inclines that are neither parallel nor perpendicular to the articular surface [1]. Zone 2 also contains a greater concentration of proteoglycans, i.e., approximately 1.5–2-fold greater than in Zone 1; correspondingly, Zone 2 is better at resisting deformation [1, 2]. In general, chondrocytes have a spherical morphology and are sparsely distributed throughout the middle zone. Zone 3, or the deep zone, tends to contain more proteoglycan content and a higher level of deposition of the thickest collagen type 2 fibrils [1]. These collagen type 2 fibrils are generally arranged in a columnar fashion, and chondrocytes are densely stacked perpendicular to the articular surface. The assembly of ECM molecules and cells within these zones creates unique microarchitectures and apertures with gradients [3]. The articular cartilage interface ends with Zone 4, itself composed of distinct tidemark and calcified zones. The tidemark serves as the chondro-osseous junction that distinguishes non-calcified from calcified articular chondrocytes and can have a thickness of up to 10 μm [14, 15]. It is primarily composed of collagen and hyaluronic acid, has a trilaminate appearance [16, 17], and provides a site for perpendicularly aligned collagen fibrils of Zone 3 to tether to the tidemark [15]. The tidemark is a metabolically active junction that is associated with endochondral ossification and long bone development in humans [16, 17]. Changes in the microanatomy of the tidemark, such as duplication of the junction, have been found to be closely associated with aging and osteoarthritis [15–17]. Zone 4 differs markedly from the other zones with respect to the mineralization of the ECM; furthermore, at this stage sparsely distributed hypertrophic chondrocytes can be observed [3]. This occurs due to both an abundance of collagen type 10 produced by hypertrophic chondrocytes and the calcification of cartilage [16]. Finally, as a transition layer between the cartilage and subchondral bone, Zone 4 is essential for dissipating mechanical forces from the bone [16].

The biomechanical properties of articular cartilage are also influenced by specific joint movements and/or articulation at the synovial joint. Synovial joints, also known as diarthrodial joints, have superior load-bearing capacity and reduce the friction between articulating surfaces during movement [5]. Articular cartilage is often housed in such joints and is usually surrounded by synovial fluid, a non-Newtonian fluid. Synovial fluid is obtained from blood plasma and comprises biomolecules including proteoglycans, collagenases, hyaluronic acid, lubricin, and prostaglandins [5]. Given these components, synovial fluid is important for maintaining the osmotic flow of water in and out of cartilage.

Since the main function of articular cartilage is to absorb and appropriately dissipate mechanical shocks, the synovial fluid acts as a lubricant, assisting normal functioning during the loading and unloading of the joints [1, 5]. Overall, the proteoglycans present in the ECM are largely polyanionic and thus repel each other, contributing to tissue elasticity and stiffness [6]. This characteristic also allows tissues to retain large amounts of water, which endows them with biphasic properties. Moreover, water retention in interstitial proteoglycan pockets is further aided by hydrophilic repulsion imparted by carbohydrate moieties present in glycosaminoglycan (GAG) molecules [6]. Previous studies have found that Zone 1 contains the highest quantity of free water but the lowest proteoglycan content. This allows for the maximum flow of fluid out of Zone 1 in response to compressive force [6]. However, Zones 2 and 3 both have relatively high bound water and proteoglycan content, which creates high hydrostatic pressure upon compression [6]. The superficial zone is essential for the lateral dispersion of shear and tensile forces along the cartilage bone boundary, which hosts the highest quantity of tangentially aligned collagen fibers [6]. In contrast, the middle and deep zones help withstand compressive forces while walking, standing, or running. These four zones working together constitute a unique system that enables a wide range of motion and flexibility during movement.

Minor alterations in the ECM of articular cartilage can exert drastic effects on joint function. Proper ECM maintenance largely depends on factors such as mitochondrial dysfunction, oxidative stress, cellular senescence, and inflammation [10]. These factors can be the result of infections, injuries, improper joint loading, or other comorbidities, including diabetes, obesity, and cardiovascular disorders [10]. Moreover, continual and prolonged dysfunction of the articular cartilage ECM can result in osteoarthritis. Osteoarthritis itself is a common tissue degenerative disorder that is associated with aging but is also known to occur in younger individuals. The severity of osteoarthritis can be assessed by evaluating signs of inflammation, osteophyte formation, and the degradation of cartilage tissue, among other factors. Although the Kellgren-Lawrence scale has traditionally been used to assess osteoarthritis progression, the International Cartilage Repair Society (ICRS) scale is now the most widely used (Fig. 3). The molecular events causing the progression of osteoarthritis can be linked to tissue inflammation, neurovascular invasion, and chondrocyte hypertrophy, all of which can lead to degradation of the joint, as shown in Fig. 4.

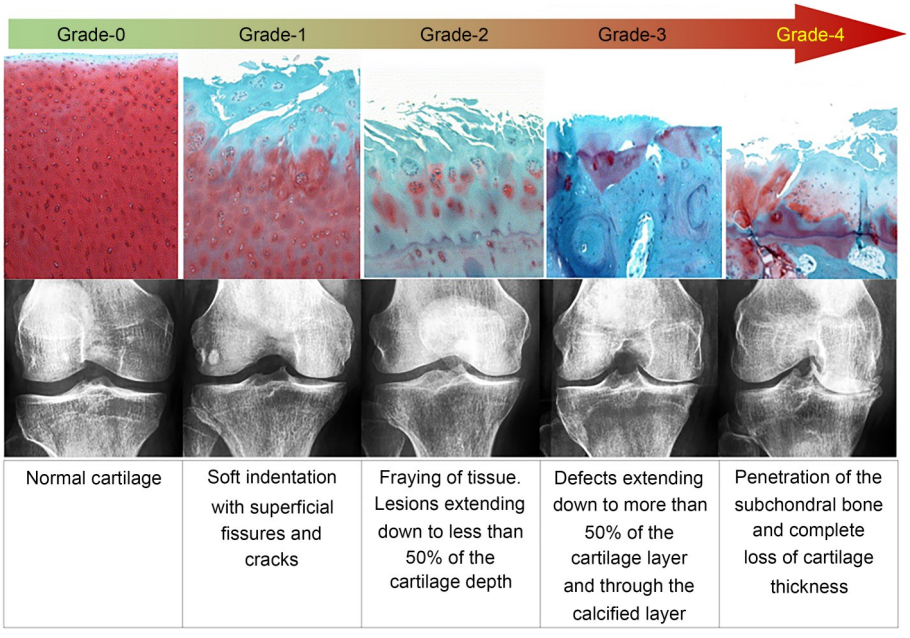

Fig. 3 The International Cartilage Repair Society (ICRS) scale permits grading the severity and progression of osteoarthritis in patients. It does so on the basis of radiological assessment and other clinical symptoms. Reproduced from [27] (Copyright 2005, with permission from OsteoArthritis Research Society International) and [28] (Copyright 2023, with permission from the authors, licensed under CC BY 4.0)

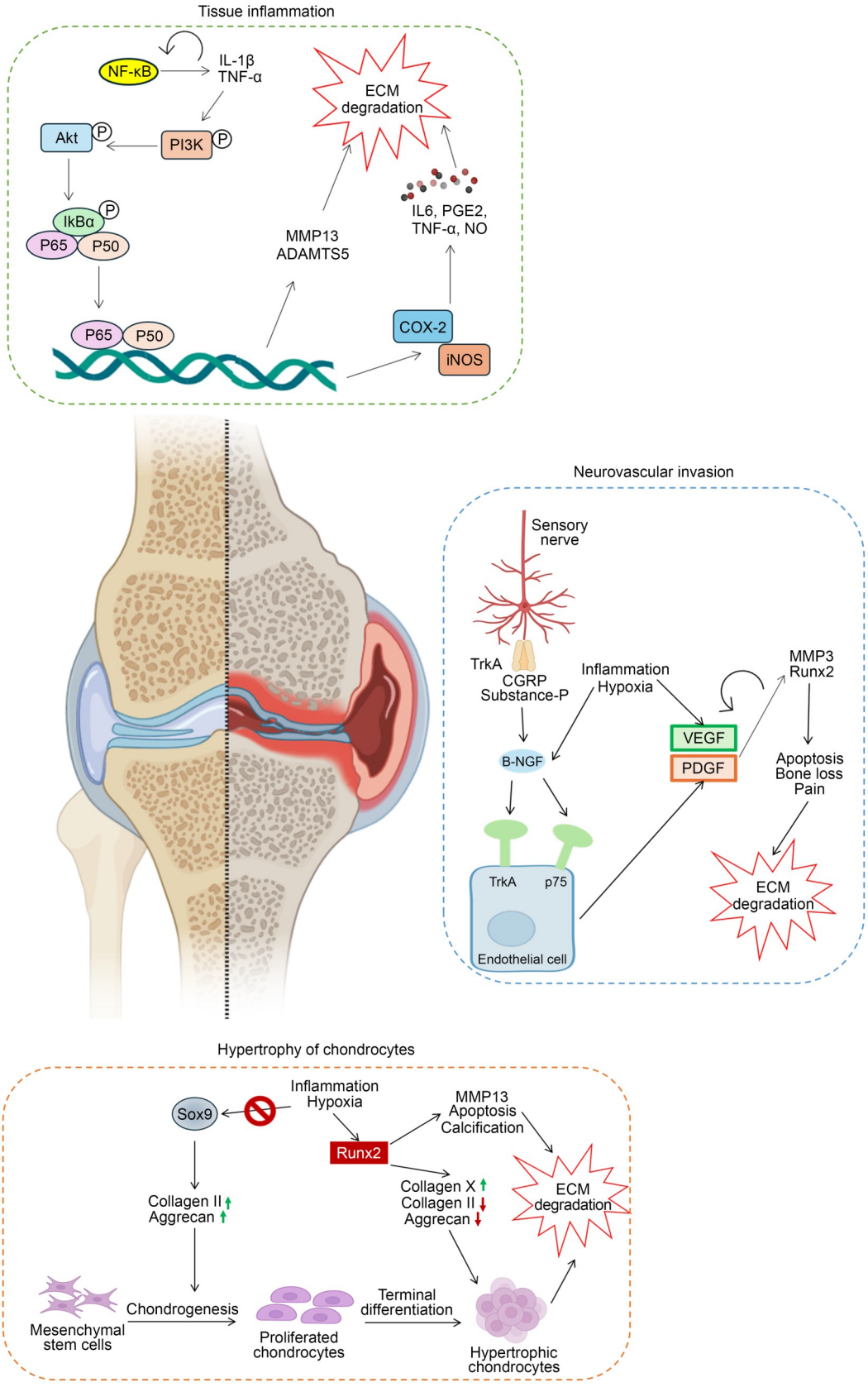

Fig. 4 Overview of key molecular mechanisms involved in osteoarthritis pathogenesis. These pathways can be triggered by factors such as aging, stress, and mitochondrial dysfunction, all of which lead to imminent breakdown of the ECM and subsequent degradation of articular cartilage joints

2.1 Tissue inflammation

The causes of inflammation in osteoarthritis patients are multifaceted and include both age-related changes and factors related to obesity. In the early stages of osteoarthritis, inflammation occurs in the synovial lining, and downstream effects begin to be observed in cartilage tissue. This includes the infiltration of lymphocytes, neutrophils, and macrophages into the synovium [18]. Lymphocytes such as LAG-3+ regulatory T cells and CD3+ T cells secrete proinflammatory cytokines such as interleukin-1 beta (IL-1β) and tumor necrosis factor-alpha (TNF-α), which combine to escalate joint inflammation, leading to greater cartilage damage and worsening conditions like osteoarthritis [18]. Cytokines not only induce the synthesis of enzymes that directly degrade cartilage, such as matrix metalloproteinases (MMPs), but also induce the production of other proteinases that increase the production of compounds such as prostaglandin E2 (PGE2) [19]. This is achieved by modulation of the expression of key enzymes and genes, including cyclooxygenase-2 (COX-2), microsomal prostaglandin-E synthase-1 (mPGES-1), and secretory phospholipase A2 (sPLA2) [19]. IL-1β is also known to inhibit the synthesis of GAGs and collagen type 2 by promoting the apoptosis of chondrocytes via the production of reactive oxygen species (ROS) [20]. Furthermore, TNF-α impairs the chondrogenic potential of cartilage tissue by inhibiting the migration of CPCs [20].

Physical stress on joints and the presence of inflammatory substances such as nuclear factor kappa-B (NF-κB) and mitogen-activated protein kinase jointly promote the activation of certain pathways inside chondrocytes [21]. Importantly, these pathways are known to be upregulated in osteoarthritis. When NF-κB is activated, the production of molecules such as MMPs, nitric oxide synthase-2 (NOS2), COX2, and IL-1β increases, and these molecules contribute to the breakdown of the cartilage ECM [21]. Consequently, this increases integrin signaling, which is triggered by the breakdown of fibronectin fragments, and integrin signaling promotes the further production of MMPs, a disintegrin and metalloproteinase with thrombospondin motifs, and chemokines, causing further damage to cartilage. Another key player in this process is a transcription factor called hypoxia-inducible factor-2 alpha (HIF-2α), which is significantly elevated in osteoarthritis and plays a crucial role during the final stage of chondrocyte maturation. HIF-2α production is upregulated in response to hypoxia in cartilage tissue, and its expression is also affected by proinflammatory cytokines such as IL-1β and TNF-α [19]. Progression to late-stage osteoarthritis is marked by cartilage degradation, increased secretion of IL-1β, IL-6, IL-8, IL-18, IL-17, IL-22, and transforming growth factor-beta 1 (TGF-β1) [18], and synovitis, which is characterized by the inflammation of the synovial membrane, resulting in joint pain, stiffness, and swelling [18].

With aging, chondrocytes within cartilage become less active, a process that is marked by increased accumulation and expression of advanced glycation end-products and their receptors [19]. This change disrupts normal signaling pathways and synthetic activity, and results in the increased production of cytokines and chemokines. In addition, the aging process is accompanied by a decrease in autophagy, a mechanism that protects against cellular stress. Overall, decreased autophagy leads to cell death, further fueling inflammation that causes osteoarthritis. In parallel, obesity has also been identified as a significant risk factor, since white adipose tissue acts as an endocrine organ that produces adipokines. Adipokines contribute to a chronic low-grade inflammatory state that can directly influence cartilage homeostasis [19]. Notably, both the infrapatellar fat pad and chondrocytes within the joint also produce adipokines, thereby perpetuating the inflammatory cascade. The stimulation of articular chondrocytes by adipokines is known to trigger the expression of MMPs and NOS2, thereby exacerbating the inflammatory environment and contributing to cartilage damage in osteoarthritis [19]. Mitochondrial dysfunction is also observed during aging and can contribute to osteoarthritis progression. An altered function of mitochondria is the upregulation of PGE2, ROS, and nitric oxide (NO), which affect adenosine triphosphate (ATP) synthesis. ATP imbalance also promotes the cycle of inflammation, oxidative stress, mitochondrial dysfunction, and, ultimately, apoptosis, thus further exacerbating osteoarthritis [22, 23].

2.2 Neurovascular invasion

Healthy articular cartilage is avascular, a fact that can be attributed to the nature of the development of cartilage from the mesenchyme [1]. Without a direct blood supply, the cartilage ECM largely relies on the synovium to obtain nutrients and oxygen via diffusion [3]. Furthermore, articular cartilage cannot transmit sensations of pain, touch, or pressure, since no nerve fibers are present. However, various glycoproteins and chondrocytes can transmit mechanosensory signals to some extent [1]. As a result, damage to articular cartilage may not cause immediate pain, as injuries to other tissues in the body normally do. The lack of innervation can also contribute to challenges in detecting early cartilage damage, since pain is generally not a direct symptom until damage progresses to affect surrounding structures with their own nerve supply, such as the bone or synovium [22].

Following damage to the joint and breakdown of cartilage tissue, the ECM is exposed to the mesenchyme; this is characteristic of Grade 3 and 4 osteoarthritis. Once this

occurs, the contact allows neurovascular invasion, a process of infiltration of nerve fibers and blood vessels into the cartilage tissue [22]. Neurovascular invasion further induces pain and impairment in osteoarthritis patients. Studies evaluating patients undergoing total knee replacement for severe osteoarthritis often show blood vessels breaking through the tidemark. Normal articular cartilage contains thrombospondin-1, troponin-1, and chondromodulin-1, all of which suppress vascular endothelial growth factor (VEGF) activity [24]. However, in osteoarthritis, these anti-angiogenic molecules and proteoglycans are degraded due to inflammation. Furthermore, due to increased HIF-2α activity, the activity of VEGF and platelet-derived growth factor increases [24]. This in turn promotes angiogenesis in damaged cartilage tissue via degradation of the basement membrane caused by the production of MMPs. VEGF also causes sclerosis of the subchondral bone by disrupting the balance between osteoclast and osteoblast activity [24]. This can result in osteophyte formation, which is further aided by increased expression of runt-related transcription factor-2 (Runx2) [24, 25].

The presence of sympathetic and sensory nerves has been reported in damaged cartilage tissue alongside vasculature. In addition, nerve fibers—both surrounding blood vessels and free-floating—and nerve trunks have been found within the bone marrow beneath the cartilage (i.e., in the subchondral bone marrow) as well as inside osteophytes [22]. Beta-nerve growth factor (β-NGF) is a key factor that stimulates the growth of sensory nerves. These nerves respond to β-NGF by interacting with tropomyosin receptor kinase A (TrkA) and p75, thereby triggering sensory nerve growth [22]. Moreover, the presence of β-NGF in joint tissues can lead to both abnormal nerve growth (neuroplasticity) and increased sensitivity of nerve endings (hyperalgesia), thereby contributing to chronic pain [22]. Another pathway influenced by β-NGF involves binding with its receptor TrkA, which causes release of certain neuropeptides called substance-P (SP) and calcitonin gene-related peptide-I (CGRP-I) [22]. These neuropeptides bind to specific receptors on endothelial cells, thereby stimulating angiogenesis.

2.3 Chondrocyte hypertrophy

After inflammation-mediated degradation of cartilage tissue, the formation of hypertrophic chondrocytes is another hallmark of osteoarthritis progression [26]. The molecular signaling pathways involved in this process can be linked to natural processes of bone and cartilage formation that occur during development. Chondrogenic differentiation is closely linked to bone formation, since they share a common osteochondral progenitor that arises from MSCs [26]. Here, the key signaling molecules governing chondrogenic differentiation and proliferation are Runx2 and sex-determining region Y-box 9 (Sox9). Sox9 serves as a central regulator of chondrogenesis, whereas Runx2 expression is suppressed in healthy cartilage [26–28].

Within the cartilage tissue itself, chondrocytes themselves express Sox9, which in turn activates genes encoding crucial ECM proteins such as collagen type 2 and aggrecan [28]. Overall, direct control of bone morphogenetic protein (BMP) activity is crucial for cartilage maintenance, since it prevents the dedifferentiation of chondrocytes into osteogenic mesenchymal progenitors and inhibits the expression of Runx2. Runx2 acts as a master switch to initiate hypertrophic differentiation [27]. In osteoarthritis, Sox9 expression is decreased, possibly due to inhibitory effects induced by hypoxia and inflammation [28]. The upregulation of Runx2 is associated with increased activity of the HIF-2α, NF-κB, and wingless-related integration site (Wnt)/β-catenin pathways [27]. This upregulation results in the production of enzymes such as MMP9, MMP13, a disintegrin and metalloproteinase with thrombospondin motifs 4 (ADAMTS4), ADAMTS5, ADAMTS7, and ADAMTS12, all of which contribute to cartilage breakdown [26]. In addition, the formation of fibrocartilage, a tissue with mechanically inferior properties, is observed. Interestingly, cells expressing high levels of Runx2 also display characteristics that resemble cellular senescence, including an enlarged, flattened morphology and increased staining for β-galactosidase, a marker of senescence. In one recent study, this process was found to rely on p53 signaling pathways [27]. Due to the degradation of cartilage caused by MMPs, degraded products are released into the synovial fluid, reducing its viscosity and impairing lubrication efficiency [29]. The degraded products can also activate macrophages present within the synovial fluid, thereby further amplifying the production and activity of inflammatory cytokines [30].

In addition to disrupting signaling and promoting the formation of hypertrophic chondrocytes, osteoarthritis prevents the differentiation of MSCs from the exposed mesenchyme toward chondrogenic lineages [26]. It also promotes focal calcification of the cartilage ECM, tidemark duplication, and the formation of osteophytes or bone spurs due to increased turnover of mineral content [26]. Furthermore, when the long bones of a person with osteoarthritis rub together during normal movement, damage can be caused to the subchondral area due to the lack of robust load-bearing articular cartilage tissue [26]. This damage further exacerbates joint inflammation and the subsequent vascularization that accompanies it. Overall, the pathophysiology of osteoarthritis highlights the intricate relationship between inflammation, matrix degradation, and disruption of signaling pathways involved in cartilage maintenance and repair. Thus, understanding the key molecular mechanisms regulating the articular cartilage microenvironment remains

highly important for improving osteoarthritis treatments. Such an understanding may enable researchers to identify and design improved treatment modalities for clinical application.

3 Clinical products currently available for cartilage tissue engineering

With the emergence of tissue engineering in regenerative medicine, understanding its three key pillars—i.e., scaffolds, cells, and biomolecules—remains important. Scaffolds are networks of polymeric (or less commonly, other) biomaterials that provide a surface for cells to adhere to and proliferate on. Furthermore, depending on the scaffolding technique, various microarchitectures, mechanical stabilities, and functionalities can be achieved [31]. The most common scaffolds used for tissue engineering include fibrous, porous, decellularized extracellular matrices, and hydrogels.

Fibrous scaffolds are characterized by the presence of aligned fibers, which mimic fibrous ECM components such as collagen, elastin, and fibrin, all of which have nanofibrous structures [31]. Fibrous scaffolds are generally fabricated via techniques such as electrospinning and melt spinning [31], and these materials can achieve different structural complexities while providing excellent tensile properties. For example, fibrous scaffolds have been widely used for skin, cartilage, cardiac, and vascular tissue engineering [31]. In one study, screw-based extrusion electrospinning (SBEE) was shown to achieve fine deposition of biomaterials of varying viscosities [32]. Moreover, SBEE can be used to load bioactive factors and nanoparticles that can aid in tissue regeneration [32, 33]. Erisken et al. loaded varying concentrations of β-tricalcium phosphate (β-TCP) nanoparticles along with polycaprolactone (PCL) to fabricate a continuous gradient nanofibrous scaffold that could mimic the cartilage-bone interface [32]. In a later study, Erisken et al. loaded varying combinations of insulin and β-glycerophosphate (β-GP) with PCL to target cartilage regeneration by promoting chondrogenic differentiation of stem cells [33]. In general, porous scaffolds provide a larger surface area for cells to adhere to, since there is high interconnectivity among pores present within the scaffolds. Such scaffolds can be fabricated via techniques such as freeze-drying, gas foaming, and solvent casting [31], with cubic, gyroid, and spherical pore geometries capable of being obtained with tunable pore dimensions and overall porosity [34]. Interestingly, pore geometry has proven to be essential for mimicking the cell–cell interactions of mechanobiologically active tissues such as bone and cartilage [34]. A correct 3D pore geometry can also aid in the transport of minerals, nutrients, and ECM components [29, 34]. Decellularized extracellular matrices (dECMs) can be obtained by processing donor tissue in specific ways to retain extensive protein and macromolecular networks and to eliminate cellular components [32]. Decellularization of the ECM can be performed via various physical, chemical, and enzymatic methods [32].

Hydrogels are 3D biphasic scaffolds that can hold large amounts of water [31]. Hydrogels can be fabricated via various methods, including chemical crosslinking, enzymatic crosslinking, coacervation, free-radical polymerization, and freeze-thawing [31]. Once prepared, hydrogels form intricate porous structures that can hold a large amount of fluid, making them highly suitable for housing cells. Furthermore, they can easily mimic native tissue architectures, making them the first choice for regenerating cartilage tissue [31]. For example, hydrogels have traditionally been employed to treat defects in cartilage tissue engineering applications. Finally, hydrogels are commonly fabricated using biomaterials such as collagen, chitosan, and polyethylene glycol (PEG), among others.

Biomaterials are generally categorized as natural or synthetic based on their source. Various biomaterials used in cartilage tissue engineering are listed in Table S2 (supplementary information). In general, natural biomaterials are preferred because they are biocompatible, do not often cause severe immunogenic reactions, and are biodegradable [32]. They have also been found to promote cell signaling pathways and cell adhesion [32]. However, scaffolds fabricated using only natural biomaterials may not possess good mechanical properties and have processing limitations [32]. These drawbacks can be addressed by using synthetic biomaterials. Overall, synthetic biomaterials are less expensive than natural biomaterials and do not degrade as easily; this is usually preferable for tissues, which can take a very long time to regenerate [32]. While synthetic biomaterials have a lower innate ability to promote tissue remodeling, they can be chemically functionalized to do so. Biomaterials can also be functionalized by surface modification methods such as chemical etching, peptide grafting, and plasma treatment. For example, PCL is a synthetic biomaterial that is hydrophobic and therefore shows poor cell adhesion [35]. However, surface etching with sodium hydroxide (NaOH) can be used to hydrolyze ester bonds into carboxyl and hydroxyl groups, thus providing sites for cell adhesion [35]. Arg-Gly-Asp (RGD) peptide has also been grafted onto biomaterials such as polycarbonate urethane to promote the adhesion of cells to the biomaterial and to prevent apoptosis [36]. Finally, nitrogen ion plasma treatment has been successfully used with silk fibroin films to increase cell adhesion and proliferation [37]. Here, surface oxidation via plasma treatment allows for covalent immobilization of ECM biomolecules [37].

Furthermore, scaffolds can be classified as acellular or cellular. Acellular scaffolds are directly applied to the

defect site and do not contain any cells. Instead, they depend on cell infiltration from the surrounding tissue post-implantation. In contrast, cellular scaffolds are encapsulated with cells during or after fabrication, and the scaffold is then cultured under ambient conditions to facilitate the attachment and growth of cells prior to implantation. Many unique scaffolds are commercially available for treating osteoarthritis in humans. However, these scaffolds must undergo rigorous clinical trial testing and receive approval from government organizations such as the U.S. Food and Drug Administration before they are available clinically. During clinical trials, scaffolds are assessed using different parameters, including tissue repair/fill volume, T2 relaxation time, visual analog scale (VAS), Western Ontario & McMaster Universities Osteoarthritis (WOMAC) index, Osteoarthritis Research Society International (OARSI) responder index, International Cartilage Repair Society (ICRS) score, International Knee Documentation Committee (IKDC) score, health-related quality of life (HRQoL), and EuroQoL-5D (EQ-5D) questionnaire, among other measures. See a list of criteria summarized in Table 1.

The immune response also plays a key role in determining scaffold biocompatibility post-implantation. Biodegradable scaffolds are known to elicit both innate and adaptive responses in humans [50, 51]. The innate response is responsible for cell signaling patterns associated with wound healing and inflammation [50, 51]. This process is mediated largely by dendritic cells, macrophages, and neutrophils [50]. However, an exaggerated innate response can interfere with collagen production and thereby promote tissue degradation [50]. The adaptive response is undertaken by T- and B-cells, both of which can induce hypersensitivity [51]. Thus, assessing the immunological response of scaffolds after implantation is essential for clinical trials. The lymphokine migration test (LMT) can be used to measure the levels of pro-inflammatory cytokines such as ILs, TNF-α, and interferons (IFNs), all of which are released by lymphocytes [52]. Importantly, the sensitivity of LMT is 95.2%, and the specificity is limited to 76.9% [52]. Thus, a better method of gauging the immune response to implanted scaffolds in osteoarthritis patients is to perform cytokine profiling of the synovial fluid. In such a test, pro-inflammatory cytokines like IL-1β, TNF-α, and IL-6, and anti-inflammatory cytokines like IL-1 receptor antagonist (IL-1RA), IL-4, and IL-10 can be used as biomarkers to determine the severity of the immune response [53]. Moreover, proteins like S100 calcium-binding protein A12 (S100A12), MMP1, and MMP13 can be used as biomarkers [53, 54]. Finally, synovial fluid can be collected from patients and tested using antibody arrays, enzyme-linked immunosorbent assays, or human cytokine assays [53].

3.1 Viscosupplementation

Articular cartilage is a gel-like material that contains an interconnected collagen fiber network. This network is bound to large aggrecan assemblies via hyaluronic acid motifs. In osteoarthritis, the hyaluronic acid degrades, which disrupts joint loading and unloading. Thus, many injectable hydrogels have been fabricated using hyaluronic acid, collagen, or their derivatives to supplement damaged tissue. This method of treatment is known as viscosupplementation. It is minimally invasive, and the hydrogel can be directly injected into the treatment site. These treatments provide temporary relief and must be administered periodically to maintain the optimal viscosity and function of the joint [55]. However, viscosupplementation can be ineffective for treating chondral lesions and full-depth osteochondral defects.

3.1.1 Atelocollagen®

Developed in 1986, Atelocollagen® was the first tissue-engineered product capable of treating cartilage defects. Aqueous collagen is dispersed in a pH- and osmolality-adjusted buffer containing glucose and phosphate-buffered saline (PBS) [56], which allows Atelocollagen® to be injected at the defect site, where it boosts healing by participating in signaling to various cells necessary for tissue recovery. The efficacy of intra-articular Atelocollagen® injection has been studied in male New Zealand white rabbits [57]. In this study, at 12 weeks, a 2 mm chondral defect had completely healed, and fully integrated articular cartilage had formed [57]. In 2021, a double-blind, randomized, controlled clinical trial was performed in 200 patients to assess the efficacy of injecting Atelocollagen® to relieve joint pain [58]. The authors administered a single dose of 3 mg/mL via intra-articular injection in patients with osteoarthritis below Grade 3 [58]. Follow-up was performed for both treatment and placebo groups at 4-, 12-, and 24-week post-injection. Patients in the treatment group reported improvements in VAS, WOMAC, and 36-item short-form health survey (SF-36) scores [58]. However, it is unclear whether this treatment aids in the regeneration of articular cartilage tissue.

3.1.2 HYMOVIS®

HYMOVIS® or high-molecular-weight viscoelastic hyaluronan, is an 8 mg/mL formulation dissolved in the PBS of HYADD4®, a hyaluronic acid (HA)/amide derivative, in which 2%–3% of the carboxyl groups present in the polymer are modified by introducing hexadecylamine as side chains via amide bonds [59]. This HA/amide derivative is a partially hydrophobized HA and is reported to form a physical hydrogel in an aqueous medium. The impact of HYMOVIS®

Table 1 Standardized tests and scoring systems used to assess pain, functionality, and tissue repair in osteoarthritis patients undergoing knee surgery. Most clinical trials use a combination of these tests to quantify treatment efficacy

Name	Details	Scoring system (if any)	Reference
Visual analog scale (VAS)	Pain scores self-reported by individuals on a handwritten 10-cm line ranging from "no pain" on the left end (0 cm) and "worst pain" on the right end (10 cm)	0–2: no pain; 2–4: mild pain; 4–6: moderate pain; 6–8: intense pain; 8–10: excruciating pain	[38]
Western Ontario & McMaster Universities Osteoarthritis (WOMAC) index	Applied to assess osteoarthritis in the hip and knee; including a questionnaire consisting of 24 items	Three subscales: pain (5 items): related to climbing stairs, standing, etc.; stiffness (2 items): after first waking and later in the day; physical function (17 items): involving activities like bending, heavy household work, etc.	[39]
Osteoarthritis Research Society International (OARSI) responder index	Measuring the percentage of patients experiencing significant improvement in symptoms related to osteoarthritis; patients being classified as "responders" if they meet scoring criteria	Patients being classified as "responders" based on improvement in pain scores, improvement in physical function (measured using validated scales and questionnaires), and overall patient assessment	[40]
International Knee Documentation Committee (IKDC) score	A structured questionnaire is used to gather information about the patient's knee-related symptoms and function to understand the patient's knee condition	Symptom assessment is done based on swelling, stiffness, pain, and locking/catching sensation	[41]
International Cartilage Repair Society (ICRS) score	Specifically designed to evaluate macroscopic outcomes of cartilage repair procedures; aiming to simplify and focus the evaluation of cartilage repair on clinical needs	Degree of defect repair: 0 to 4 with 0 for no repair; integration to border zone: 4 points for complete integration and 0 points for no contact; macroscopic appearance: from 4 (smooth) to 0 (total degeneration); overall repair assessment: normal (12 points), nearly normal (11–8 points), abnormal (7–4 points), or severely abnormal (3–1 points)	[42]
Health-related quality of life (HRQoL)	Used to assess how an individual's health status impacts their overall quality of life	Four core questions on general health: physical illness, injury, mental health, and how poor physical or mental health keeps patients from performing routine activities such as self-care, work, or recreation	[43]
EuroQoL-5D (EQ-5D)	A versatile tool standardized for measuring health-related quality of life; the "5D" in its name referring to its use of five dimensions for describing health state: mobility, usual activities, self-care, pain & discomfort, and anxiety & depression	Each dimension has five levels of severity: no problems; slight problems; moderate problems; severe problems; extreme problems	[44]
Magnetic resonance observation of cartilage repair tissue (MOCART) score	A system developed to standardize the evaluation of cartilage repair using magnetic resonance imaging (MRI); helping clinicians evaluate the success of cartilage repair techniques and monitor patient recovery progress	The following parameters are assessed: degree of defect repair; integration to the border zone; surface integrity; subchondral bone changes; repair tissue signal intensity; structure; subchondral lamina	[45]
T2 relaxation time	Used in MRI and nuclear magnetic resonance spectroscopy; describing the time it takes for the protons in a sample to realign with the magnetic field after being disturbed	The T2 relaxation time of native cartilage: (50.2±8.4) ms (for early unloading) and (51.3±8.5) ms (for late unloading)	[46]
Tegner activity score	A scale used to assess patient activity level, particularly following knee injury and during rehabilitation	Scale ranging from 0 to 10, with higher scores indicating higher activity levels	[47]
Knee injury and osteoarthritis outcome score (KOOS)	A self-administered questionnaire used to monitor disease course and outcomes following surgical, pharmacological, and other interventions	Containing five subscales: (1) pain; (2) other symptoms; (3) activities of daily living; (4) sport and recreation function; (5) knee-related quality of life; each subscale is scored separately from 0 (extreme knee problems) to 100 (no knee problems)	[48]
36-Item short form health survey (SF-36) score	A widely used questionnaire designed to measure general health status of patients; consisting of 36 questions and providing scores across eight health domains	Scores are aggregated into two summary measures: physical component summary and mental component summary (MCS), each of which ranges from 0 to 100, with higher scores indicating better health	[49]

was examined via the use of synthetic calcium pyrophosphate (CPP) crystals to stimulate a monocytic cell line (THP-1) in in vitro models [60]. The authors found that HYMOVIS® significantly inhibited IL-1β production and displayed anti-inflammatory properties by reducing IL-8 release (i.e., from (2300±315) to (150±35) pg/mL) and inhibiting the migration of polymorphonuclear cells. The suppression of IL-8 release was further confirmed following stimulation with lipopolysaccharides [60]. HYMOVIS® was tested in a multi-center open-label clinical study to treat knee osteoarthritis [61]. In that trial, two doses of HYMOVIS® were given to the patients one week apart, and a follow-up assessment was performed after one year. While the authors found significant improvement in WOMAC and EQ-5D scores over time, 26% of patients experienced continued progression of osteoarthritis [61].

3.1.3 Synvisc-One®

Synvisc-One® (Hylan G-F 20) is an injection that supplements the fluid in the knee to help lubricate and cushion the joint and is capable of providing up to six months of osteoarthritis knee pain relief [62]. The injection includes hyaluronic acid and a pharmaceutically acceptable carrier with which the hyaluronic acid is crosslinked by cyclizing a double bond in a moiety of cinnamic acid in a partially amidated hyaluronic acid [62]. An in vitro study assessed how Synvisc-One® affected the health and growth of chondrocytes taken from the knee joint of osteoarthritis patients [62]. The authors used both 2D (flat) and 3D (spheroid) models to mimic the cartilage environment, and these samples were exposed to Synvisc-One® at two different concentrations, after which cell growth and viability were measured. Compared with an untreated control, Synvisc-One® at both concentrations (i.e., 100 and 500 μmol/L) improved the viability and growth of chondrocytes in a 2D culture for up to 72 h. In 3D culture, Synvisc-One® at 500 μmol/L improved the survival and maintenance of chondrocytes after seven days [62]. A randomized, double-blind, multi-center clinical study was thereafter performed using Synvisc-One® to treat patients with knee osteoarthritis [63]. In that study, a single dose of Synvisc-One® was injected intra-articularly and the effects were followed for 26 weeks. The authors found that this treatment improved OARSI and WOMAC scores, although a significant placebo effect was also observed [63].

3.1.4 EUFLEXXA®

EUFLEXXA® is a viscoelastic, sterile solution containing highly purified, high-molecular-weight hyaluronan in PBS [64]. It is administered as a 1% sodium hyaluronate injection extracted from bacterial cells. It is indicated for treating pain in patients with osteoarthritis of the knee who have failed to respond adequately to conservative non-pharmacologic therapy or simple analgesic treatment [64]. A randomized, double-blind, multi-center clinical study was conducted in patients with chronic osteoarthritis; in this trial, three weekly intra-articular injections of EUFLEXXA® were given, and patient status was assessed at 26 weeks [64]. Here, 47% of patients reported that they were pain-free after the treatment, a finding that was supported by low VAS scores [64].

3.2 Implantable scaffolds

Implantable scaffolds are prefabricated and can be monophasic or multiphasic, depending on their composition and method of fabrication. In general, these scaffolds are fabricated via traditional tissue engineering techniques such as freeze-drying. They can also be composed of hydrogels, which can be crosslinked either beforehand or in situ at the implantation site. Moreover, since these scaffolds do not contain any cells, they depend on the infiltration of MSCs from the bone marrow to initiate chondrogenic differentiation and facilitate tissue regeneration. Therefore, implantation is often performed alongside surgical procedures such as mosaicplasty or debridement, both of which are highly invasive.

3.2.1 CartRevive™

The CartRevive™ scaffold is a relatively new monophasic scaffold. It is a blend of dextran and hyaluronic acid conjugates developed by a Dutch bioengineering company called Hy2Care® [65]. To use this scaffold, an injection site is first debrided, and then the hydrogel is injected and crosslinked in situ via a quick enzymatic reaction. Amine-terminated dextran/tyramine conjugates are then grafted onto hyaluronic acid via 1-ethyl-3-(3-dimethylaminopropyl) carbodiimide (EDC)/N-hydroxysuccinimide (NHS) [65]. In one study, Jin et al. studied the efficiency of CartRevive™ as an injectable scaffold in vitro [66]. They found that the HA/dextran/tyramine conjugate could mimic the structure of proteoglycans found in natural cartilage. When bovine chondrocytes were placed in the CartRevive™ scaffold, they remained alive, as confirmed by a live/dead assay. In addition, these hydrogels promoted increased chondrocyte growth and matrix production relative to those containing only dextran/tyramine composites [66]. At present, the CartRevive™ implant is undergoing human clinical trials to treat mild cartilage defects.

3.2.2 ChonDux™

ChonDux™ is an adhesive hydrogel composed of photo-crosslinkable PEG combined with functionalized chondroitin

sulfate [67]. Polyethylene glycol diacrylate (PEGDA)-HA is the main component of hydrogels with methacrylated chondroitin sulfate (CSMA), which serves to covalently bridge PEGDA-HA and the tissue surface [67]. During clinical trials, ChonDux^{TM} was applied by accompanying debridement and microfracturing. The site of injury was first debrided before undergoing microfracturing to allow MSCs to inhabit the application site. The PEGDA-HA hydrogel was then injected and photopolymerized in situ. This protocol enabled MSCs to be trapped within the hydrogel while simultaneously being bridged to the tissue surface via CSMA [67]. A follow-up study involving 18 patients was performed to assess the efficiency of ChonDux^{TM} treatment during repair of a full-depth cartilage defect of 2–4 cm^2 over the course of two years [68]. After microfracturing, a CSMA pregel was used to fill the defect volume entirely; this was then exposed to ultraviolet (UV) light for 240 s to form a hard hydrogel. Postoperatively, patients received rehabilitation for 12 weeks, after which they were barred from engaging in high-impact resistance activities and exercise after one year [68]. Patients reported low VAS scores at four days, seven days, and six weeks post-operation. Moreover, T2 relaxation time and tissue repair volume analyses were performed using magnetic resonance imaging (MRI) every three months for up to two years. The authors found that T2 relaxation time decreased to normal levels by 12 months and remained stable for the remainder of the study. Finally, a tissue repair volume of (94.2± 16.3)% was reported by the end of the study [68]. However, cartilage delamination (in 27% of patients) and osseous overgrowth (in 22% of patients) were both reported during this study [68].

3.2.3 MaioRegen^{TM} Prime

MaioRegen^{TM} Prime is a triphasic scaffold sold by JRI Orthopedics Ltd. (UK) that aims to treat lesions in patients with ICRS Grade 4 osteoarthritis [69, 70]. Biphasic variations of the same product are also sold for chondral and osteochondral defects. The first phase of MaioRegen^{TM} Prime comprises collagen type 1 sourced from equines and targets chondral regeneration [69]. The second and third phases are made of collagen type 1 and magnesium-hydroxyapatite (Mg-HAp) at 60:40 and 30:70 ratios, respectively [69]. The second phase aims to regenerate calcified cartilage and the subchondral bone plate, whereas the third phase aims to regenerate the spongy bone layer. In 2011, a pilot clinical study was conducted to test the biomimetic potential of this product in 30 patients, with a two-year post-op follow-up performed for 28 patients [70, 71]. During the study, the implantation site was exposed via parapatellar arthrotomy, and sclerotic tissue was eliminated. The scaffold was then implanted, and patients were provided with rehabilitation for up to 7–8 months. The IKDC and Tegner scores of patients clearly improved by the two-year follow-up. However, many adverse events were reported during MRI analysis via MOCART score testing. For example, 20% of patients experienced hypertrophy in adjacent cartilage tissue, 63% had cleft formation, and 47% had fissures and ulcerations on the surface of the repaired tissue [71]. Another clinical study was conducted in 2017 on 27 patients. Here, the scaffold was adhered to the implant site via fibrin glue to provide additional stability; the authors performed a five-year follow-up [72]. The IKDC and Tegner scores of the patients had significantly improved by at least twofold by the five-year follow-up. However, 38.9% of patients experienced hypertrophic cartilage, 44.4% had cysts, edemas, and sclerosis of the subchondral bone, and 27.8% had cleft formation in repaired tissue.

3.2.4 TruFit®

TruFit® is a biphasic bioresorbable plug developed by Smith and Nephew that targets full-scale osteochondral defects. The first phase is designed to facilitate cartilage regeneration and involves the fabrication of poly(lactic-co-glycolic acid) (PLGA)/poly glycolic acid (PGA) at a ratio of 3:1 [73]. The second phase focuses on bone regeneration and is composed of calcium sulfate ($CaSO_4$) [73]. Upon implantation, pluripotent osteoprogenitor cells are siphoned into a porous plug. A clinical study in which TruFit® plugs were implanted in 10 patients reported that full integration was observed in only three patients by a two-year follow-up [74]. For the remaining seven patients, cystic lesions were observed in the subchondral bone. Furthermore, the two-year post-op IKDC score was only 57.4. Other clinical studies have reported the formation of fibrous scar tissue, incomplete integration of the plug, and low EQ-5D scores in patients switching to arthroplasty or mosaicplasty following implantation of the TruFit® plug [75].

3.2.5 ChondroMimetic®

ChondroMimetic® is a biphasic scaffold manufactured by TiGenix [76]. The first phase, which targeted bone regeneration, was performed using bovine collagen type 1 and chondroitin sulfate resuspended in HAp. A second phase targeting cartilage regeneration was performed using porcine collagen type 2 and chondroitin sulfate. In the liquid phase, there is interdiffusion between both phases, and this can mimic the tidemark region upon freeze-drying. The freeze-dried scaffold was then crosslinked with EDC and NHS. An open-label single-center extension clinical study has been conducted on 17 patients to assess the long-term feasibility of ChondroMimetic® for the treatment of osteochondral defects <12 mm [77]. During this study, scaffolds

were implanted at mosaicplasty donor sites. At an eight-year follow-up, a lesion fill volume of (95.2±3.6)% was reported, with a T2 relaxation time of (52.5±4.8) ms [77].

3.3 mACI-based scaffolds

Autologous chondrocytes are the most popular choice for fabricating cellular scaffolds for osteoarthritis treatment and are known as autologous chondrocyte implants. The chondrocytes used for this treatment are usually harvested from non-load-bearing cartilage tissue and thereafter expanded in vitro. mACI is the third generation of ACI in which autologous chondrocytes are integrated with a scaffold before implantation (Fig. 5). This allows the scaffold to have zero immunogenicity; however, it also poses a risk of dedifferentiation and donor site morbidity. While autologous chondrocytes are popular for cartilage tissue engineering, MSCs have also been used. MSCs can easily be harvested from a patient's infrapatellar fat pad, periosteum, peripheral blood, or synovial fluid. Moreover, induced pluripotent stem cells (iPSCs) generated from patient cells can be used; however, they pose risks of possible tumorigenicity and unpredictable cellular reprogramming. Finally, products such as Zofin™ and MIUChon™ are approved iPSC-based injections but do not contain scaffolding biomaterials.

3.3.1 Hyalograft® C

Hyalograft® C is a modified hyaluronic acid membrane seeded with autologous chondrocytes that was introduced by Fidia Advanced Biopolymers in 1999. This membrane was fabricated via Hyaff-11®, a benzylic ester of HA, that imparts a fibrous structure to the scaffold [78]. It allows for slower resorption—i.e., for up to four weeks—than HA, which is degraded in three days. A retrospective cohort clinical study was performed on 141 patients with a three-year post-op follow-up [79]. In this study, autologous chondrocytes were seeded onto a membrane before being implanted at the site after arthrotomy. The membrane was adhered to the surface using fibrin glue for larger defects. An 18-month post-op biopsy revealed the formation of hyaline-like tissue along with some fibrocartilage. Although the IKDC score at 38 months post-operation was (78.6±20.2)%, graft failure was reported in 10 patients [79].

3.3.2 BST-CarGel®

BST-CarGel® is composed of chitosan and forms a hydrogel under physiological conditions [80]. Chitosan not only aids during the differentiation of MSCs into chondrocytes but also helps retain the spherical morphology of cells

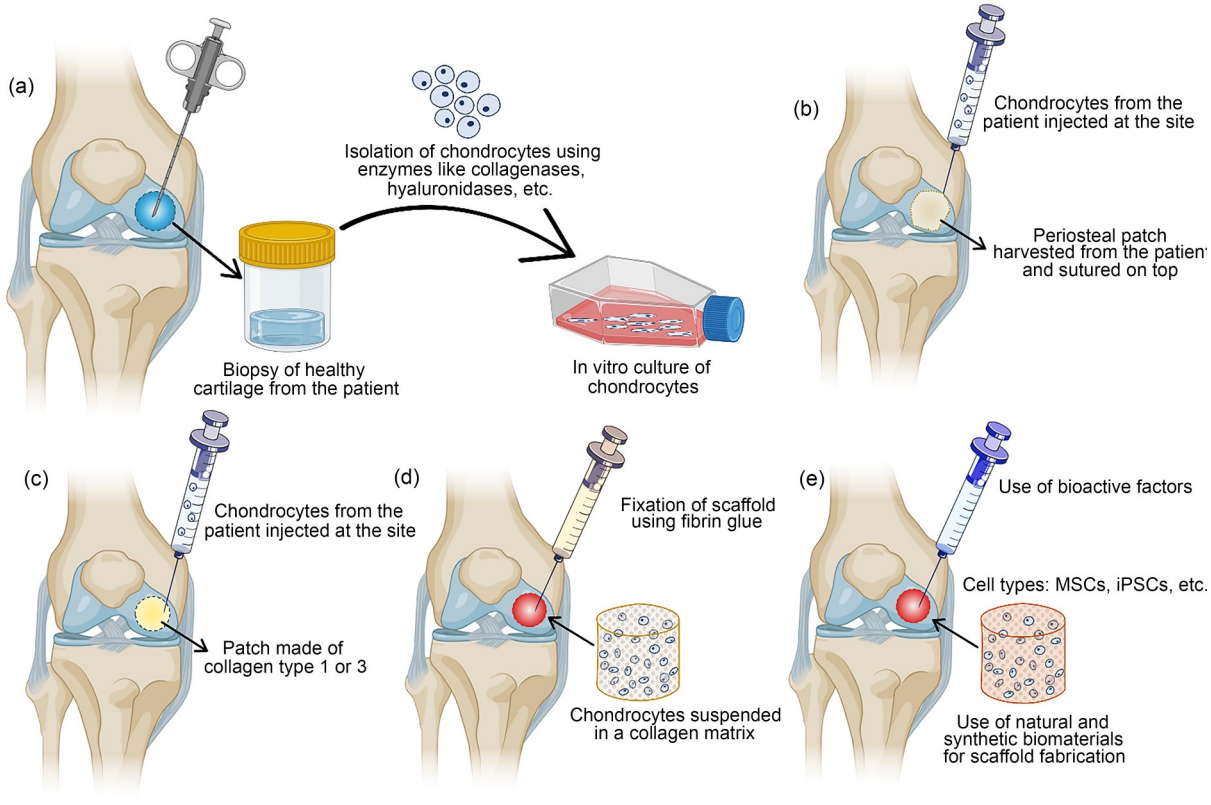

Fig. 5 A depiction of the key features of autologous chondrocyte implantation (ACI) and matrix-assisted ACI (mACI)-based scaffolds. (a) Overview of processes commonly used for the isolation and expansion of autologous chondrocytes. Illustrations of the various generations of ACI—the first (b), second (c), third (d), and fourth (e) generations. (d, e) Overview of mACI

within the ECM. BST-CarGel® is composed of chitosan with varying degrees of deacetylation ranging from 30% to 70% [80]. This unique chitosan composition forms a hydrogel at 37 °C and pH 7.4, with acetylated and deacetylated chitosan molecules having molecular weights in ranges of 10–4000 kDa and 200–20 000 Da, respectively [80]. Overall, the unique composition of this hydrogel provides excellent lubrication. A randomized controlled trial was conducted to test the efficiency of BST-CarGel® compared with microfracture alone over 12 months [81]. In this study, 41 subjects with a singular symptomatic focal lesion on their femoral condyles were injected with BST-CarGel® after microfracturing, whereas another 39 patients were only treated with microfracture. BST-CarGel® was prepared using whole autologous peripheral blood at a 3:1 ratio and was applied to the lesion after microfracturing. In the group that received the BST-CarGel® treatment, (92.8±2.0)% of lesions were filled after 12 months, whereas in the microfracture-only group, only (85.2±2.1)% of lesions were filled [81]. Furthermore, the T2 relaxation time of the BST-CarGel® treatment group ((49.1±6.9) ms) was very close to that of native cartilage.

3.3.3 CARTISTEM®

CARTISTEM® is a hydrogel composed of MSCs and HA for patients with severe knee osteoarthritis [82]. To develop this hydrogel, MSCs were obtained from allogenic human umbilical cord blood (hUCB) and expanded to obtain only mononuclear MSCs. hUCB-MSCs were used since they do not elicit immunogenicity and can be easily cultured. An open-label, single-arm, single-center clinical study was then performed in seven patients, and a seven-year long-term follow-up was performed for six patients [82]. The application site was exposed via arthrotomy to create multiple holes of 5 mm in depth. A single dose of CARTISTEM® containing 2.5×10^6 cells was applied to the lesions. The VAS score decreased significantly by three months post-op but gradually increased at six months and remained constant until the seven-year follow-up. Similarly, the IKDC scores of patients reached a peak at six months and one year post-op but decreased marginally by the seven-year mark. Furthermore, arthroscopic examination of the regenerated tissue at one year post-op revealed the formation of hyaline-like cartilage with a high GAG content [82].

3.3.4 CaReS®

The cartilage regeneration system or CaReS® is a collagen type 1 implant containing autologous chondrocytes. Collagen type 1 is purified from rat-tail tendons and is mixed with chondrocytes to obtain a final 3 mg/mL mixture [83]. This mixture was then allowed to polymerize naturally at 37 °C to obtain implants with a cell density of 3×10^4 cells/implant or more. Next, an open-label exploratory clinical trial was conducted in patients suffering from ICRS Grade 3 and 4 osteoarthritis [83]. At 52 weeks post-operation, patients reported a mean IKDC score of 74.1, a VAS score of 22.9, and a T2 relaxation time of (60.4±7.3) ms. While complete integration was observed in six of seven patients, the authors also observed frequent complications during wound healing. Moreover, joint effusion was observed in five patients [83].

3.3.5 NeoCart®

NeoCart® is a collagen type 1 implant for treating chondral defects in patients with ICRS Grade 3 osteoarthritis [84]. During administration, the implant is seeded with autologous chondrocytes before being cultured in a bioreactor to promote a hyaline-like phenotype. Culturing implants in a bioreactor provides pressure and oxygen tension conditions that mimic the native articular cartilage joint microenvironment [84]. Before implantation, the sulfated GAG content was estimated to ensure a minimum concentration of 10 mg/mL. In a 2009 study, eight patients were treated with NeoCart®, and six of these reported a 67%–100% defect fill volume at a two-year post-operation MRI scan [84]. A randomized controlled clinical study then compared the effects of NeoCart® treatment and microfracture in 30 patients [85]. In this trial, the NeoCart® group consisted of 22 patients. The implantation site was exposed via arthrotomy, and the scaffold was secured via a bioadhesive. At five years post-operation, few differences were reported in the IKDC and VAS scores of the two experimental groups.

3.3.6 Cartipatch®

Cartipatch® is a hydrogel plug for osteochondral defects that comprises autologous chondrocytes suspended within an alginate−agarose mixture [86]. This product was developed to address the drawbacks associated with injecting a chondrocyte suspension at the site itself, e.g., leaking cells and chondrocyte dedifferentiation. For this trial, 200–300 mg of cartilage tissue was harvested from each patient and then expanded as a monolayer culture for three passages [86]. Next, approximately 1×10^7 cells/mL were harvested and used to prepare the final product. An initial multi-center clinical study was performed using ICRS Grade 3 and 4 osteoarthritis patients [86]. By the two-year follow-up appointment, hyaline-like cartilage regeneration was observed in approximately 62% of the patient group. A subsequent multi-center, randomized, and controlled clinical study was performed to compare the efficiency of Cartipatch® with mosaicplasty in 76 patients diagnosed with ICRS Grade 3 and 4 osteoarthritis. This study also compared methods for small ($\leqslant$3.5 cm^2) and large defects (>3.5 cm^2) and featured

a two-year follow-up [87]. In the Cartipatch® group, anteromedial arthrotomy was performed to implant the product, whereas in the mosaicplasty group, osteochondral tissue plugs were harvested from the non-load-bearing region of the femur and then implanted at the defect site via parapatellar arthrotomy. All patients received heparin treatment for 30 d and were allowed to resume normal weight-bearing activities two months post-operation. While the Cartipatch® group reported higher IKDC scores than the mosaicplasty group pre-operation, upon post-operation follow-up, the mosaicplasty group reported a greater increase in IKDC scores [87]. Furthermore, in the Cartipatch® group, intra-articular effusion (in six patients) and hematoma (in two patients) were reported in trial subjects.

3.4 Limitations of available clinical products to treat osteoarthritis

Traditionally, tissue engineering techniques such as freeze-drying and solvent-casting have been used to fabricate clinical products for osteoarthritis treatment. However, performance data reveal critical issues that remain unaddressed, including the development of hypertrophic cartilage, the formation of mechanically inferior tissue, and the prevalence of inflammation. The integration of scaffolds into native tissue can also be improved. The fabrication of cartilage tissue presents unique challenges, particularly regarding the achievement of proper mechanical properties dictated by the organization of collagen and proteoglycans. This mechanical integrity is crucial for tissue functionality, especially for weight-bearing joints such as the knee [88]. While different polyesters can be used to modify scaffold mechanical strength and degradation rate, there remains a risk of inflammation, which can strongly impact implant success rates [89]. At present, clinical methods mainly target pain management and often fail to provide satisfactory results. However, synthetic scaffold materials may have well-defined structures that may not permit full cellular colonization. For example, a knitted poly-L-lactic acid (PLLA) scaffold has large open areas that are not covered by the scaffold, and this can lead to cells adhering mainly to the surface rather than filling the scaffold space. Thus, limited colonization can impact treatment effectiveness, since cells may not be able to fully interact with the scaffold for tissue regeneration [89]. While natural polymers such as collagen are attractive for cartilage repair, they also present key challenges. Obtaining sufficient porosity and interconnectivity in collagen scaffolds is crucial for cell colonization and tissue ingrowth. Thus, the limited availability of native collagen type 2 poses challenges for scaffold design despite the availability of recombinant options [88, 89].

Another challenge in cartilage tissue engineering involves inflammation at the transplant site. Inflammatory cytokines, especially IL-1β and TNF-α, are implicated in cartilage destruction. Studies have shown that osteoarthritic synovium-derived medium and inflammatory cytokines can inhibit MSC chondrogenesis, thereby impacting engineered cartilage tissue inside the body. These challenges arise post-transplantation and can also lead to tissue fibrosis and the formation of fibrochondrocytes rather than articular cartilage. Insulin-like growth factors (IGFs) such as IGF-1 and IGF-2 are known to be expressed within chondrocytes, where they orchestrate chondrocyte proliferation and foster differentiation of MSCs toward the chondrocyte lineage. Transforming growth factor-β (TGF-β) has emerged as a pivotal factor for orchestrating MSC differentiation into chondrocytes, potently stimulating cellular proliferation and augmenting the synthesis of the ECM while inhibiting endochondral ossification. Within the expansive TGF-β superfamily, BMPs including BMP-2, GDF-5, and BMP-7 play key roles in chondrogenesis and terminal differentiation, where they significantly enhance collagen synthesis and formation of the cartilage matrix. Furthermore, fibroblast growth factors are required to maintain cartilage matrix homeostasis and to activate stem cells. Finally, the regulatory protein VEGF has also emerged as a critical factor for supporting endochondral bone formation and potentially modulating chondrocyte proliferation within cartilaginous tissue [90]. In general, each of these challenges can be mitigated by incorporating novel drugs and growth factors that can reduce inflammation and promote chondrogenesis.

A major barrier to translating tissue-engineered cartilage into the human knee is maintaining reliable and consistent chondrogenic tissue over time. Relative to chondrocytes, stem cells have a greater proliferative ability. Therefore, using chondrocyte-based cell numbers for stem cell treatments may not accurately measure the optimal cell density required [91]. While research on modified scaffolds remains ongoing, newer tissue engineering techniques such as 3D printing and bioprinting have also become clinically relevant, since bioprinting can produce scaffolds with superior architecture and optimal porosity. Furthermore, many biomaterials and cells can be used to bioprint intricate structures while incorporating anti-inflammatory drugs or growth factors that promote chondrogenesis. This makes bioprinting a suitable method for designing next-generation osteoarthritis treatments.

4 Advances in bioprinting technologies for cartilage tissue engineering

3D printing is a popular technique used in additive manufacturing. Bioprinting is a subtype of 3D printing that uses bioinks to fabricate 3D structures. The core principle

involved in bioprinting is to build the final product layer by layer [92]. However, factors such as porosity and mechanical strength must be considered during the scaffold design to ensure long-term efficiency [92]. A key component of bioprinting involves designing the printed scaffold, which can be performed via computer-aided design software such as SolidWorks, AutoCAD, Autodesk® Fusion 360, and/or Computer Aided Three-Dimensional Interactive Application (CATIA). These programs are generally used to sketch models in a 2D plane that can then be rendered to obtain 3D designs. The resulting 3D designs are then exported as a standard tessellation language file that can be further processed using slicing software such as Simplify3D, UltiMaker Cura, Prusa Slicer, and KISSlicer. Slicing software packages generate a geometric code (G-code) file that comprises a set of coordinates determining the pattern of movement of a 3D printer nozzle. Various parameters such as flow rate, temperature, and layer height can also be varied depending on the type of material used and design of the model.

4.1 Bioprinting strategies

Many different types of 3D printing exist, including fused-deposition modeling (FDM) and selective laser sintering; however, not all of them can be used for bioink printing, since bioinks contain cells. The subsets of 3D printing that can be used successfully for bioprinting are shown in Fig. 6.

4.1.1 Inkjet-based bioprinting

Inkjet 3D printing was developed by Hewlett-Packard in the 1950s as a method of strategically dispensing droplets of ink via thermal, piezoelectric, or electrostatic actuators [93]. Inkjet-based bioprinting is also known as drop-on-demand bioprinting, since the ejection of droplets can be finely controlled according to printing needs [93]. Additional customization can be achieved by varying the types of actuators used. For thermal inkjet-based bioprinting, the actuator is heated to 250–350 °C for a short period to facilitate bubble formation in the bioink [94]. This quick expansion and contraction of the bubbles at the nozzle helps a bioink droplet move toward the outlet for deposition [94, 95]. In piezoelectric inkjet-based bioprinting, varying voltage pulses are applied to a piezoelectric actuator element near the nozzle [96]. This results in deformation in the outlet chamber, thus ejecting the bioink droplet [95, 96]. Similarly, in electrostatic inkjet-based bioprinting, nozzle deformation is obtained by applying electricity to a pressure plate via an electrode [94]. Overall, inkjet-based bioprinting is a high-throughput method that can generate high-resolution prints with droplet diameters ranging from 10 to 2000 μm [94]. Furthermore, a wide range of biomaterials can be employed using this method to bioprint different types of cells.

4.1.2 Extrusion-based bioprinting

Extrusion is the most popular method of bioprinting and has been in continuous use since the 1980s [93]. In this method, the bioink is extruded through the nozzle head by applying a systematic load on the chamber containing it [93, 97]. The load application within the chamber can involve a pneumatic, piston, or screw mechanism [93, 97]. In general, extrusion-based bioprinting can be easily customized to suit individual bioinks and their unique characteristics. Specific customizations include varying nozzle gauges, flow rates, print speeds, rates of extrusion, and printing temperatures, among others [97].

4.1.3 Stereolithography (SLA)-based bioprinting

SLA-based bioprinting employs a layer-by-layer approach using biomaterials or bioinks that can be exclusively photo-crosslinked. For example, bioinks such as PEGDA and gelatin methacryloyl (GelMA) are commonly used, since they can be crosslinked when exposed to UV or visible light [98]. Photoinitiators such as benzophenone and lithium phenyl-2,4,6-trimethylbenzoyl-phosphinate (LAP) are also frequently used to assist with crosslinking [98]. The bioink is held in a tank that is free to move along the *Z*-axis, thereby allowing the print to build the required height layer by layer [98], while a digital micromirror device projects light and can move along both the *X*- and *Y*-axis [99]. This allows for the direct projection of light in patterns that can be specified via G-codes [99].

4.1.4 Light amplification by stimulated emission of radiation (LASER)-assisted bioprinting

LASER-assisted bioprinting is another additive manufacturing technique that uses LASER as an energy source to deposit biomaterials onto a suitable substrate. A LASER is a collimated beam of monochromatic electromagnetic radiation that can be produced for wavelengths ranging from the infrared, UV, or visible light parts of the electromagnetic spectrum [100]. The first generation of LASER-assisted bioprinting was LASER-guided direct writing (LGDW), a technique in which a bioink suspension was exposed to a weak LASER. LGDW allowed for micropatterning of bioinks with particles having diameters ranging from 0.1 to 100 μm [101, 102]. The need for increased cell viability, resolution, and precision led to the development of LASER-induced forward transfer (LIFT). The key components of a LIFT setup include a LASER generator and a bioink transfer module [102]. The bioink transfer module includes a ribbon attached to a layer of bioink that is targeted by the LASER based on patterns specified by G-codes.

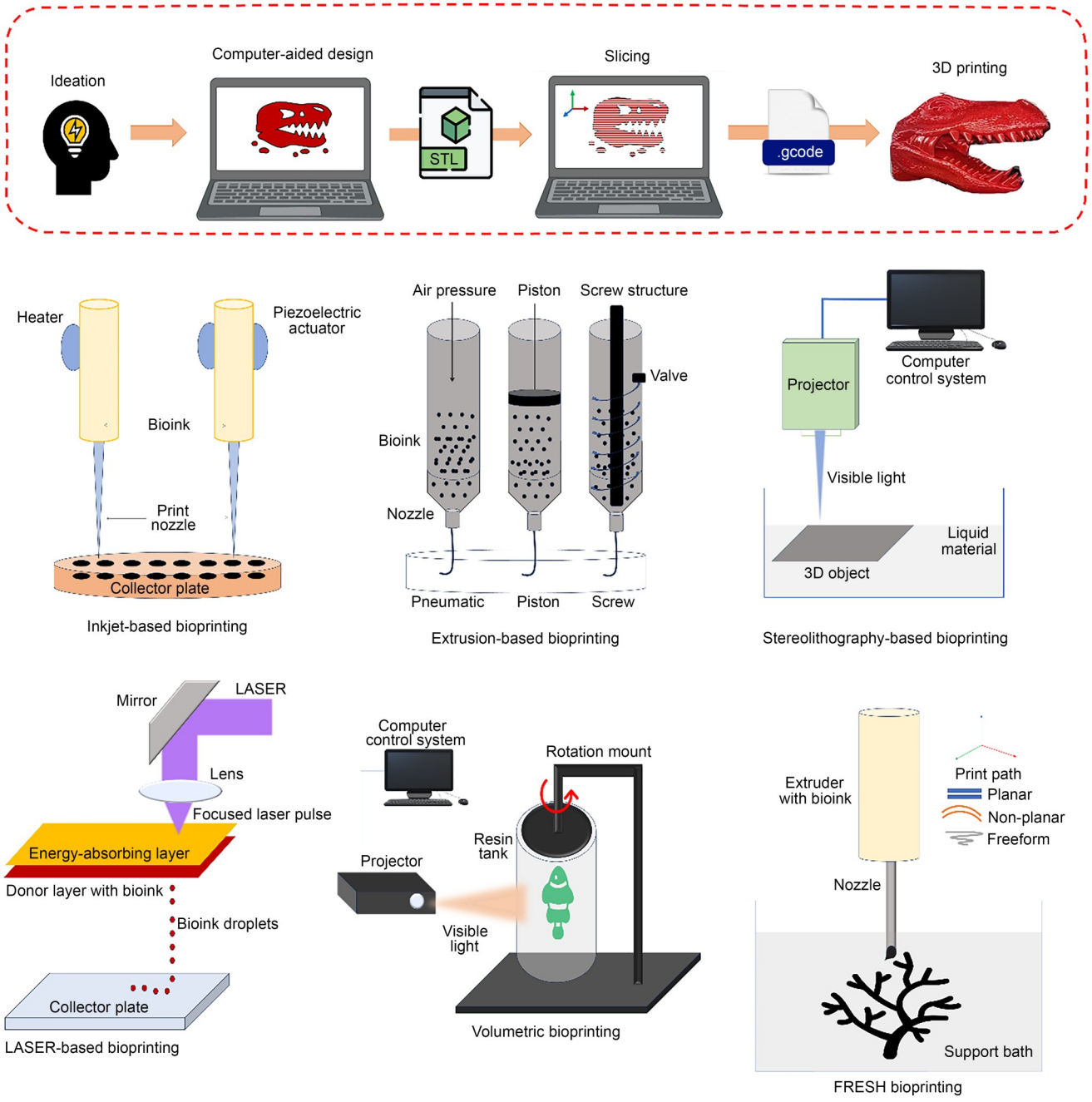

Fig. 6 Illustration of the basic workflow of 3D printing and the most commonly used types of bioprinting

4.1.5 Volumetric bioprinting

Volumetric bioprinting is a newer technology that uses photosensitive bioinks to generate scaffolds. Specifically, cell-laden photosensitive bioinks, or bioresins, are held in a vat, where they are strategically exposed to visible light to induce polymerization [103]. Unlike SLA-based bioprinting, volumetric bioprinting does not follow the layer-by-layer process of building a scaffold. Instead, the vat is irradiated with light from multiple angles to create dynamic patterns [104]. This makes it possible to fabricate centimeter-scale designs with a resolution of up to 50 μm [105]. Although resins such as acrylates and epoxies have been used, biocompatible materials such as GelMA and silk fibroin have also been used [105]. For example, Bernal et al. fabricated cell-laden GelMA hydrogels that could be printed in 12.5 s with a cell viability of >85% [106]. One of the advantages of following the "layer-less" approach is the ability to print entire tissues and organs instantaneously without generating supports or overhangs, which significantly reduces post-processing time and waste [103–105]. The resolution of the print obtained depends on image acquisition quality, which

is usually achieved by taking computed tomography scans of target tissues [103].

4.1.6 Freeform reversible embedding of suspended hydrogel (FRESH) bioprinting

In 2015, a new method of performing embedded bioprinting of hydrogels was reported by Bhattacharjee et al., Highley et al., and Hinton et al. [107–109]. This new technique is now known as FRESH bioprinting [109, 110]. In FRESH bioprinting, both synthetic and natural biomaterials are first deposited in a support bath [110]. The support bath is made of a material with Bingham plastic-like rheological behavior such as agarose, alginate, carbopol, elastomers, gelatin, nanoclay, Pluronic F-127, or xanthan gum [110]. This allows a bioink to be deposited into the support bath using a nozzle that can move and extrude in planar, non-planar, and freeform paths without disturbing previously fabricated structures, after which the bioink is cured or crosslinked. Various crosslinking strategies can be employed, including ionic, pH, enzymatic, thermal, click-chemistry, and photo-crosslinking protocols [110]. Thus, FRESH bioprinting is quickly becoming popular for the printing of soft tissues with high resolution and accuracy. Prominent companies such as Advanced BioMatrix, Inc. have created Lifeink® and LifeSupport®, a collagen-based bioink and support bath material.

4.2 Bioprinted scaffolds for osteoarthritis treatment

Bioprinting techniques have been successfully used to print a variety of different tissues. However, their suitability for osteoarthritis treatment remains a complex topic. This can be attributed to the unique architecture of the knee joint and its distinctive microenvironment. Although at present there are no bioprinted products available on the market that are specifically designed for osteoarthritis, extensive research is being conducted to develop new treatments of this kind. Design strategies can be used for chondral or osteochondral defects based on the severity of osteoarthritis as determined by the ICRS grading scale. These are summarized in Table S3 (supplementary information).

4.2.1 Chondral defects

Chondral defects are characteristic of low-grade osteoarthritis. Defects can manifest as fissures or cracks, and can result in damage to up to 50% of the total cartilage tissue. However, in general no damage is observed to the calcified Zone 4 or subchondral bone. Bioprinted scaffolds targeting chondral defects aim to regenerate hyaline cartilage while ensuring the production of important ECM molecules such as proteoglycans and collagen type 2. Previous studies have reported the use of a variety of cell types, including MSCs, iPSCs, and chondrocytes to treat chondral defects. The main aim of these treatments is to ensure the regeneration of articular cartilage while preventing the formation of fibrocartilage. Strategies used to treat chondral defects using bioprinting techniques can be grouped into bioink-based and scaffolding-based methods, as shown in Fig. 7.

4.2.1.1 Bioink-based methods

In 2017, Nguyen et al. investigated two bioinks that used iPSCs to generate 3D-bioprinted constructs designed to promote cartilage reconstruction. The compositions of these bioinks included nanofibrillated cellulose (NFC), alginate, and 4.6% mannitol for physiological osmolarity. The NFC was sterilized via electron irradiation, and alginate with ⩾60% α-1-guluronic acid was then added. Crosslinking was accomplished using 0.001% H_2O_2 exposure for five minutes, and the authors added an iPSC-conditioned medium from clone A2B iPSCs to facilitate increased survival. In the end, iPSCs were printed at a final concentration of 2×10^7 cells/mL in the bioink. The resulting constructs were cultured in a pluripotent medium mixed with conditioned DEF-CS™ for seven days. NFC/alginate 60/40 (mass fraction) resulted in better cell proliferation and survival and was able to maintain pluripotency. The bioprinting results also confirmed that the NFC/alginate 60/40 bioink supported iPSC survival and growth, yielding better 3D-printed constructs. Hence, this ratio was confirmed to be suitable for iPSC survival, growth, and chondrogenic differentiation. Coculturing with iChons or growth factors also resulted in hyaline-like cartilage tissue formation [111].

In 2021, Visscher et al. developed a bioink specific to auricular cartilage tissue using a cartilage-derived extracellular matrix (cdECM). In their study, 37.5 mg/mL gelatin and 3 mg/mL HA were mixed with different ratios of cdECM (i.e., 20, 30, and 40 mg/mL). GelMA alone was used as a control, and the different bioinks were blended with chondrocytes (2×10^7 cells/mL) prior to printing. Lattice- and ear-shaped cell-laden constructs were then bioprinted and exposed to UV light to induce crosslinking, thereby forming hydrogels. Characterization was performed using a trinitrobenzenesulfonic acid (TNBS) assay, and revealed that cdECM had (71±2)% methacrylation, whereas the GelMA hydrogel had (81±3)% methacrylation. Thus, compared to the GelMA hydrogel, the cdECM hydrogels showed lower swelling ratios. Moreover, scaffold stiffness improved with increasing concentration of cdECM (i.e., 20 mg/mL: (3837± 462) Pa; 30 mg/mL: (10 381±1339) Pa; 40 mg/mL: (25 050± 2573) Pa) when balanced with GelMA. Overall, the structure

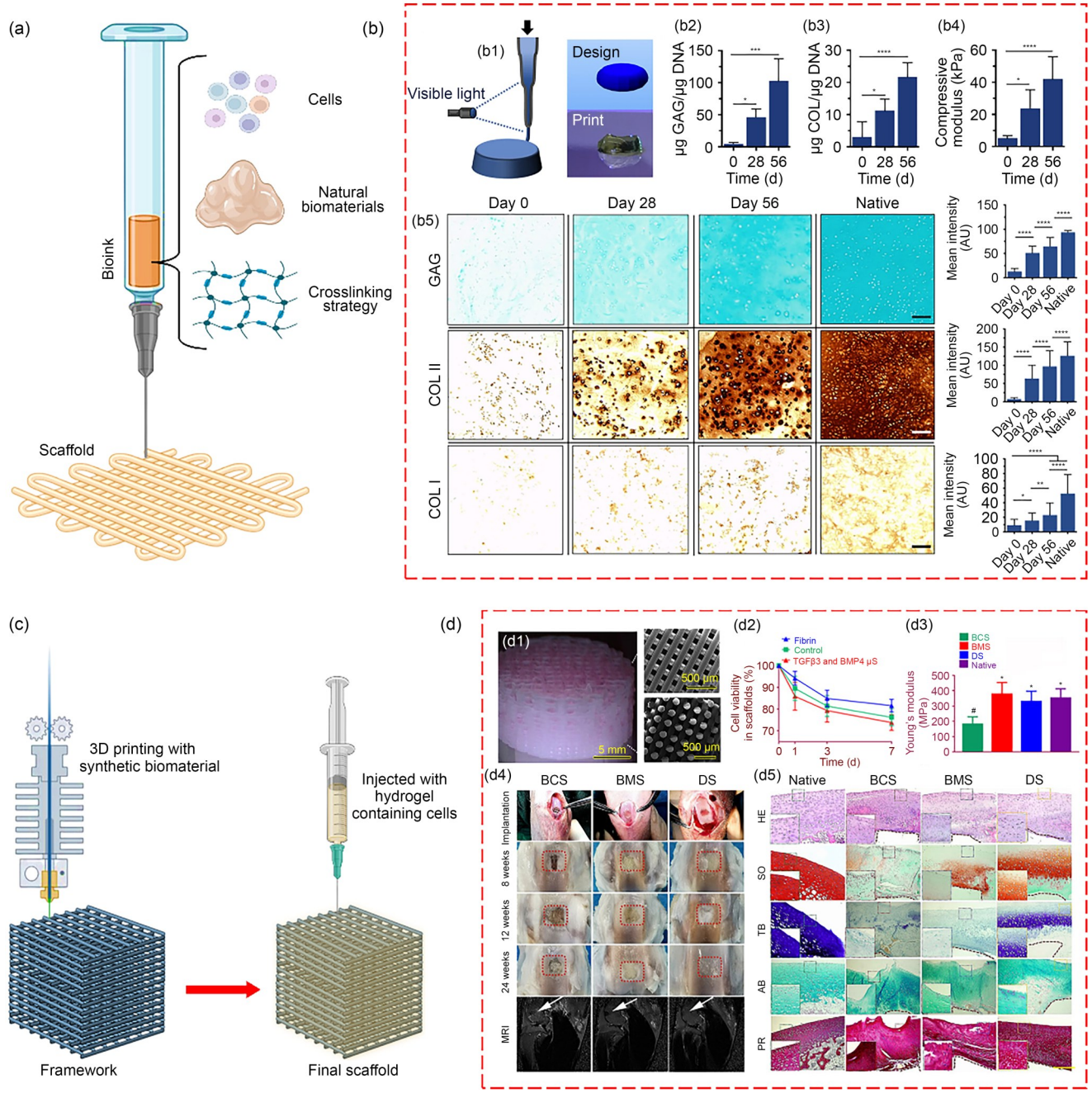

Fig. 7 Overview of bioprinting-based strategies used for the repair of partial-depth chondral defects. (a) Bioink-based methods. (b) Fabrication of non-viscous norbornene-modified hyaluronic acid (NorHA) bioink-based cartilage hydrogel using DLP-based bioprinting: (b1) representative multi-layered constructs printed via in situ crosslinking; (b2) sulfated glycosaminoglycan (GAG) content; (b3) total collagen content; (b4) compressive modulus; (b5) histological evaluation of printed constructs and their respective quantification of GAGs and collagen types 2 and 1 after 0, 28, and 56 d of culture or native bovine articular cartilage (scale bars: 100 μm; $n \geq 15$ sections, 45 images per group; $^{*}p<0.05$, $^{**}p<0.01$, $^{***}p<0.001$, $^{****}p<0.0001$). Reproduced from [114], Copyright 2019, with permission from the authors, licensed under CC BY 4.0. (c) Scaffolding-based method. (d) Fabrication of MSCs and dual factor-loaded 3D-printed gradient construct for cartilage regeneration: (d1) gross appearance of human-scale gradient scaffold with 150–750 μm spacing as analyzed via scanning electron microscopy (SEM); (d2) quantified cell viability and proliferation in printed scaffolds; (d3) Young's modulus of scaffolds relative to native cartilage after 12 weeks (data shown are mean±standard deviation (n=6); $^{*}p<0.05$ between the NG-750 group and other groups; $^{\#}p<0.05$ between the native cartilage group and other groups); (d4) scaffold implantation process and gross appearance of repaired cartilage at 8, 12, and 24 weeks (MRI was performed to image the operated knee joints (fifth row), demonstrating significantly better resolution of subchondral edemas and healing of the articular surface (white arrowheads) for joints transplanted with double stimulus (DS) scaffolds); (d5) comparison of chondroprotective effects of scaffolds measured by histological staining of repaired cartilage tissue during in vivo implantation (staining involved H&E, safranin-O (SO), toluidine blue (TB), alcian blue (AB), and picrosirius red (PR) protocols). Reproduced from [119], Copyright 2020, with permission from the authors, licensed under CC BY 4.0

and mechanical properties of the various constructs were stable. Further in vitro cell studies revealed 90% cell viability at all cdECM concentrations. Finally, the authors reported that cell proliferation within the cdECM constructs increased with increasing concentration, with 40 mg/mL resulting in significantly greater proliferation than GelMA at 1, 3, and 7 d of culturing [112].

Gomes et al. developed and characterized a bioink designed to target chondrocyte inflammation and apoptosis in osteoarthritic conditions. They did so by using different ratios of cholinium caffeate (ChC), β-(1→4)-acetylated polymannose or acemannan (ACE), and alginate [113]. The resulting bioink was prepared with 5% alginate, 5% ACE, and 1% ChC and was pre-crosslinked with 0.35% $CaCl_2$. ATDC5 cells were then integrated to create a bioink such that the final density was 8×10^6 cells/mL. Extrusion-based bioprinting was performed at 13 °C, and the scaffold was then crosslinked with 5% $CaCl_2$. The resulting bioprinted scaffold was cocultured with THP-1-activated M1 macrophages for up to seven days to simulate the inflammatory microenvironment found in osteoarthritis tissues. Ultimately, the alginate/ACE/ChC scaffold was able to successfully reduce the concentrations of TNF-α, IL-6, IL-10, and granulocyte-macrophage colony-stimulating factor (GM-CSF), thus demonstrating the efficacy of slow-release ChC in reducing inflammation. This strategy can be used to counteract inflammation in early-stage osteoarthritis, but further studies are required [113].

Extrusion-based bioprinting has been most often used to fabricate bioink-based constructs. However, this can pose challenges regarding cell viability and crosslinking. Since extrusion-based bioprinting uses pressure to force ink deposition, excessive shear stress can reduce cell viability. This can be addressed by opting for different bioprinting methods in which layer deposition occurs independently of applied pressure. For example, Galarraga et al. reported the use of a non-viscous norbornene-modified hyaluronic acid (NorHA) bioink to fabricate a scaffold using an SLA-based bioprinting approach for regenerating cartilage (Fig. 7b). This bioink comprised 2% NorHA, 0.05% LAP, and 0.08% dithiothreitol (DTT) as the macromer, photoinitiator, and crosslinker, respectively. MSCs isolated from bovine bone marrow (2×10^7 cells/mL) were then added to prepare the bioink for disc bioprinting. After 56 d of in vitro culture, the authors observed that GAG and collagen content increased approximately 100-fold and 7-fold, respectively. Furthermore, collagen type 2 deposition was found to be more common than collagen type 1 deposition, and the authors also observed the formation of hyaline-like cartilage. Although the compressive modulus at 56 d increased by about 8-fold, this was only (42.0±13.9) kPa, approximately one-tenth of that of native cartilage [114].

Some studies have reported using synthetic biomaterials together with natural biomaterials, since this approach can provide mechanical strength that is superior to constructs fabricated from natural biomaterials alone. Chen et al. conducted qualitative analyses to evaluate the proliferation potential of cartilage cells in combination with different small molecules. They found that the use of graphene oxide (GO) can help to efficiently incorporate cells into bioinks. In that study, GO was labeled with 1,1-dioctadecyl-3,3,3,3-tetramethylindocarbocyanine perchlorate (DIL), while BMP2 was labeled with fluorescein isothiocyanate (FITC), thereby permitting visualization and tracking of essential components and their use during cartilage layer reconstruction. Next, chondrocyte cell lines were cultured with GO at 37 °C and 5% CO_2. The resulting bioink was prepared using 1% collagen type 1 and 1.5% chitosan solutions at a ratio of 10:1. Next, EDC and NHS were added to collagen-chitosan and GO solutions at various concentrations (i.e., 1%, 3%, 5%, 7%, and 10%). The resulting 3D-printed tissue was then transplanted into the center of the femur cartilage via the use of a cartilage hole-drilling rat model. A Fourier transform infrared spectroscopy (FTIR) peak at 1800 cm^{-1} confirmed that carboxyl (C=O) groups played a key role in BMP2–GO interactions. Further analysis of immunofluorescence revealed that chondrocytes coexisted with GO particles, and a noticeable increase in the number of cartilage cells surrounding the GO particles was observed after 10 days. Subsequent qualitative analysis indicated that the 10% GO solution had a greater potential for chondrocyte proliferation than solutions containing lower concentrations of GO [115].

Olmos-Juste et al. studied the behavior of alginate and attempted to develop a novel bioink for the printing of 3D structures specific for treating osteoarthritis [116]. The primary aim of this study was to use waterborne polyurethane (WBPU) together with alginate to print scaffolds that can help chondrocytes maintain their distinctive shape and to promote the growth of embedded mesenchymal stem cells. WBPU bioinks containing 3.2% and 6.4% alginate were selected for extrusion-based bioprinting after loading with murine teratocarcinoma-derived chondrogenic (ATDC5) cells at a concentration of 2×10^6 cells/mL. After printing, the cell-laden scaffold was crosslinked by submerging it in 0.1 mol/L $CaCl_2$ for 5 min. After 28 d of in vitro culture, 6 μg of GAG deposition was reported with at least 10 000 chondrocytes per scaffold and no observable change to hypertrophic phenotypes. However, the deposition of collagen fibers was not detected. The alginate-WBPU bioink was found to form an aqueous polymeric system that improved the shape fidelity of the scaffold and could be used to treat chondral defects in the future [116].

In a different study, Maihemuti et al. explored the application of gelatin sourced from cold-water fishes to prepare

low-viscosity bioinks [117]. Sodium alginate was also added to the resulting bioink to enhance its mechanical strength and degradability profile. Post-printing, the scaffold was crosslinked by submersion in 2% $CaCl_2$ for 3 min and EDC/NHS at a ratio of 4:1 for another 30 min. The authors found that bioinks containing 15% gelatin and 6% sodium alginate exhibited a Young's modulus of about 22.5 MPa along with optimal printability. In vitro biocompatibility was then tested in a human chondrocyte (C28) cell line, and a near-optimal expression of aggrecan, collagen type 2, and Sox9 was detected after five days of culturing [117]. Upon in vivo implantation in Sprague–Dawley rats, biochemical analysis was performed three months post-operation to identify immunogenic reactions caused by the addition of the biomaterials. The white blood cell, red blood cell, lymphocyte, monocyte, and neutrophil counts did not significantly differ from those of the control group, suggesting a lack of immunogenicity [117]. The authors also reported that the sodium alginate and gelatin (6S/15G) formulation took 32 d to completely degrade in vivo. Furthermore, rat groups implanted with the 6S/15G scaffolds exhibited the highest ICRS score at three months post-operation, and a follow-up MRI analysis revealed maximum filling of the defect area without any complications [117].

4.2.1.2 Scaffolding-based methods

Next, we consider various methods to construct scaffolds suitable for use in osteoarthritis treatment. For example, a study in 2023 by Wang et al. focused on examining polyurethane (PU) treated with ultrasonic waves at high temperatures to improve its mechanical properties [118]. Simultaneously, an injectable gelatin/sodium alginate hydrogel loaded with 10 000 chondrocytes was prepared and crosslinked with 1% $CaCl_2$. The PU scaffold was then printed using FDM 3D printing before being ultrasonicated for 30 min, after which the hydrogel was incorporated. The resulting PU scaffold had a compressive modulus of 2.21–2.48 MPa, which is very similar to native ear cartilage. Further microscopic examination revealed the generation of new cartilage cells between the tissue and scaffold. Taken together, these findings underscore the potential of engineered scaffolds for effectively repairing damaged articular cartilage [118]. Moreover, while exclusively using biomaterials has proven to be effective in facilitating the growth of hyaline-like cartilage, the use of growth factors can help accelerate this process.

In 2020, Sun et al. studied dual growth factor release in 3D bioprinting to generate a 3D-bioprinted anisotropic cartilage construct, as shown in Fig. 7d. This construct was formed by mixing hydrogels containing cells with biological polymers and was used to print specific articular joint structures. PCL was thermally processed at approximately 60 °C to generate a physical gradient support structure, while an MSC-laden hydrogel was maintained at approximately 37 °C. Recombinant human transforming growth factor-beta-3 (rhTGFβ3) and rhBMP4 were then microencapsulated in PLGA (50:50 PLA/PGA) microspheres (μS) to facilitate the slow delivery of TGFβ3 (20 ng/mL) and BMP4 (100 ng/mL) from within the hydrogel. This composite was precisely deposited into microchannels interfaced with PCL fibers via purpose-built syringes, and the authors then tracked the release profiles of TGFβ3 and BMP4 from PLGA microparticles for 60 d. By the seventh day, the PLGA-rhodamine microparticles exhibited a uniform distribution within the hydrogel between PCL fibers, with negligible cell toxicity. The expression of two lubrication markers, collagen type 2 and proteoglycan-4, was found to be notably greater in superficial layers with small pore sizes, which resembled the pattern observed in native cartilage. In addition, the gradient scaffold is in principle capable of providing anisotropic chondrogenesis in different layers, thereby mimicking native articular cartilage. Finally, the scaffold also permits nutrient supply and vessel growth in deep layers, both of which are crucial for successful cartilage regeneration [119].

In another study, Wang et al. explored 3D-printed applications of polyglycerol sebacate (PGS) alongside a gelatin/chondroitin sulfate (CS) hydrogel for regeneration of the chondral layer of cartilage [120]. To do so, a 50% (0.5 g/mL) PGS solution was dissolved with sodium chloride (NaCl) particulates in tetrahydrofuran (THF) to obtain an ink for extrusion-based 3D printing. NaCl was then removed by freeze-drying and washing to generate a porous surface within the 3D-printed scaffold [120]. Next, a 1:1 ratio of gelatin and CS was prepared in which the porous PGS scaffold was soaked, and a combination of 0.5% EDC and 0.3% NHS was used to crosslink the hydrogel to the scaffold. The resulting composite PGS/gelatin/CS scaffolds had (592.09±22.5) μm macropores and compressive moduli of (2.443±0.071) MPa and (0.315±0.019) MPa under dry and wet conditions, respectively [120]. These scaffolds retained their shape for up to four weeks in vitro and facilitated neocartilage formation, as determined via GAG content, collagen type 2, safranin-O, and hematoxylin and eosin (H&E) staining. One week post-implantation in New Zealand white rabbits, regenerated cartilage tissue was found to have a compressive modulus of (1.801±0.149) MPa and filled (62.74±4.46)% of the original defect site [120]. Compared with native cartilage, the regenerated cartilage was (88.80±6.40)% thicker, but was also smoother and more homogeneous. These results show that the composite scaffold was successful in regenerating robust neocartilage tissue at the site of the defect; however, long-term validation studies are still required.

4.2.2 Osteochondral defects

Osteochondral defects are characteristic of high-grade osteoarthritis. At the point of defect formation, more than 50% of total cartilage tissue is damaged, with significant damage having occurred at the calcified zone and the subchondral bone. Bioprinted scaffolds targeting osteochondral defects aim to regenerate hyaline cartilage and subchondral bone while ensuring proper zonal regeneration, i.e., to mimic the native joint. Studies have reported that the effectiveness of MSCs depends on MSC migration from the mesenchyme post-implantation. The strategies used to treat osteochondral defects using bioprinted scaffolds can be categorized into bilayered and trilayered scaffolds (Fig. 8), which we discuss in greater detail below.

4.2.2.1 Bilayered bioprinted scaffolds

Nordberg et al. reported the successful generation of a 3D-printed scaffold to repair osteochondral defects in Yucatan minipigs. In this study, PCL (100%) was used to fabricate the chondrogenic phase, and 80% PCL/20% TCP was used for the osteogenic phase. An electrospun layer of 80% PCL/20% TCP was sandwiched between these layers to mimic the tidemark. Next, calcium was steadily released from the scaffolds over 28 d of in vitro culturing, with release rates leveling off after the first two weeks. The bone architecture of scaffold-treated groups resembled autologous explants, possibly due to the PCL scaffold. These scaffolds were integrated with native bone, and the autologous explant bone was indistinguishable from native bone and exhibited minimal changes over time. Moreover, cartilage matrix staining revealed no cartilage within the scaffold component of the defect. Subchondral bone porosity was then observed in scaffold-treated groups, and bone formation was successfully observed. Finally, tidemark formation was also observed in an animal model, and it was found to prevent the formation of bone tissue within the cartilage layer. Taken together, these data suggest that while scaffolds facilitated bone ingrowth and integration, cartilage formation was limited, and autologous explants performed best with respect to cartilage repair [121].

In 2021, Zhang et al. combined dECM and silk fibroin (SF) to 3D print a scaffold designed to replicate the natural structure of osteochondral tissue (Fig. 8b). These bilayered scaffolds were printed using PCL for the bone layer and a dECM/SF bioink for the cartilage layer. Compared with cartilage layer constructs, bone layer constructs exhibited slower degradation rates due to the PCL frame and greater compressive strength. Moreover, these scaffolds were designed to encapsulate growth factors. TGF-β1 release from the cartilage layer was found to promote increased expression of collagen type 2, aggrecan, and Sox9, all of which are essential for cartilage formation. Next, BMP2 release from the bone layer promoted increased expression of COL I, Runx2, osteocalcin (OCN), and alkaline phosphatase (ALP), all of which are important for bone formation. Overall, this study showed excellent integration and regeneration in a rabbit osteochondral defect model, and therefore highlights the potential of similar scaffolds as novel methods of achieving effective osteochondral tissue reconstruction [122].

In another study, Gu et al. reported the fabrication of a bilayer scaffold via digital light processing (DLP)-based bioprinting [123]. Here, the bioink used consisted of lyophilized 15% GelMA combined with 0.1% LAP and 200 μmol/L kartogenin. Kartogenin was contained only in the upper layer of the structure to promote the exclusive growth of cartilage. Furthermore, radially emanating lotus pores of 200 μm in diameter were punched in the upper layer to promote cell infiltration. The scaffold was then tested in vivo in a rabbit model via implantation in the knee. The regenerated tissue was tested, and the authors observed the distinct formation of two layers with articular cartilage at six weeks post-operation as well as new bone at 16 weeks post-operation. Moreover, at 16 weeks post-operation, the reduced modulus of the regenerated tissue was (6.32±0.45) GPa, whereas the compressive modulus of the scaffold before implantation was (302.0±15.0) kPa. These results, which show good scaffold performance overall, were primarily due to the availability of two distinct environments for defects, which is desirable for the development of osteochondral tissue [123].

Xu et al. have reported the development of a strontium copper tetrasilicate/β-tricalcium phosphate (Wesselsite ($SrCuSi_4O_{10}$)/$Ca_3(PO_4)_2$, WES-TCP) composite scaffold that was loaded differentially with chondrocytes and rabbit bone mesenchymal stem cells (rBMSCs) to aid in osteochondral regeneration [124]. In this study, a 2% WES-TCP scaffold was fabricated using extrusion-based 3D printing by mixing with 20% poloxamer. The resulting WES-TCP scaffold displayed superior mechanical properties, with a compressive strength and modulus of 16.78 MPa and (151.03±8.59) MPa, respectively [124]. Furthermore, the sustained release of Si, Sr, Ca, Cu, and P promoted the osteogenic differentiation of rBMSCs in vitro, as verified by the upregulated expression of Osterix (Osx), Sox9, and Runx2 when measured on Day 7. Moreover, chondrocyte proliferation within the chondral layer was increased, as indicated by the upregulation of collagen type 2, aggrecan, and Sox9. Further in vivo studies revealed that significant osteochondral regeneration occurred by 12 weeks post-operation; however, further analyses should be performed to confirm these results [124].

In another study, Effanga et al. reported the use of a PCL electrospun layer sandwiched between 3D printed layers of the chondral and subchondral zones [125]. A gelatin and

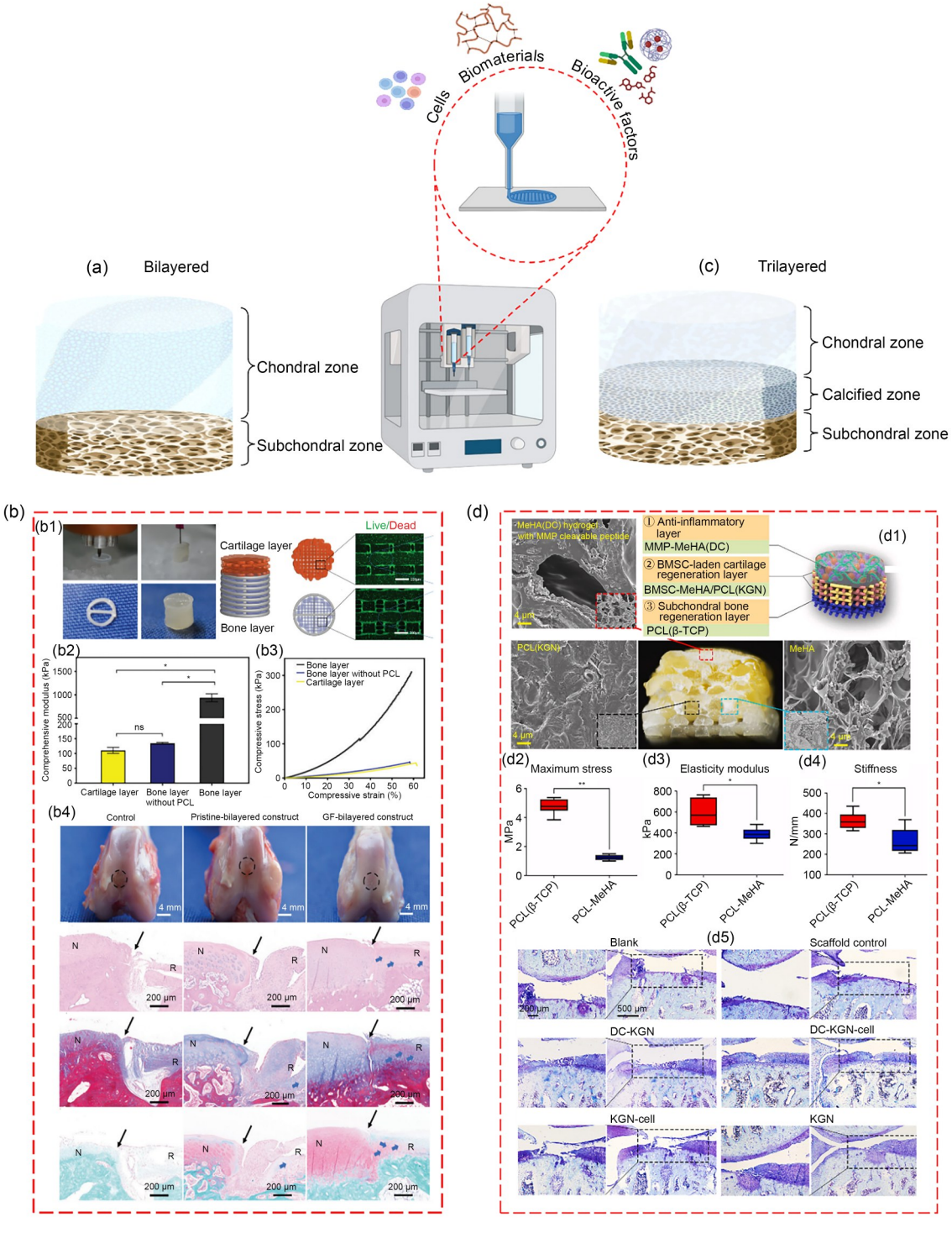

Fig. 8 Overview of bioprinting-based strategies used for the repair of full-depth osteochondral defects. (a) Bilayered bioprinted scaffold. (b) Overview of the 3D printing strategy used to fabricate a bilayered scaffold with dECM bioinks: (b1) live/dead cell viability measurements of the cartilage (top) and bone (bottom) layers; (b2) comprehensive modulus (n=3; $^{*}p$<0.05); (b3) stress–strain curves; (b4) gross observations of defect repair at three months for control, pristine-bilayered construct, and growth factor (GF)-bilayered construct groups (scale bar: 4 mm), stained with H&E, Masson's, and safranin-O/fast green. Reproduced from [122], Copyright 2021, with permission from the authors, licensed under CC BY 4.0. (c) Trilayered bioprinted scaffolds. (d) Overview of the fabrication strategy of the trilayered construct: (d1) cross-sectional views of the PCL(β-TCP) and BMSC-laden PCL-MeHA layers of the biomimetic multiphasic scaffold; (d2) maximum stress; (d3) elasticity modulus; (d4) stiffness; (d5) representative TB-stained tibial plateau images of the injured joint from different groups (data were analyzed by an independent-samples t-test (n=6); $^{*}p$<0.05, $^{**}p$<0.005). Reproduced from [128], Copyright 2021, with permission from Elsevier Ltd.

oxygenated alginate (Gel/OxAlg) ink was used for the chondral layer, and a Gel/OxAlg/HAp ink containing 3.5% (mass fraction) of hydroxyapatite (HAp) was incorporated to form the subchondral layer [125]. After 3D printing of the subchondral layer using Gel/OxAlg/HAp ink, a fibrous mesh 5–10 μm thick was deposited via electrospinning [125]. This was followed by 3D printing of the chondral layer using Gel/OxAlg ink. After fabrication, the scaffold was crosslinked via cryogelation followed by treatment with glutaraldehyde. The resulting fabricated osteochondral unit was able to withstand compressive stress up to (2.7±1.8) MPa at a strain of (37.3±3.8)%. In addition, the compressive modulus and stiffness of the scaffold were measured as (0.07± 0.05) MPa and (5.60±2.85) N/mm, respectively. Furthermore, rat mesenchymal stem cells (rMSCs) were cultured in media along with osteogenic induction of cells and scaffold. Measured cell viability of the construct with the electrospun PCL interface was more than 85% on Days 3 and 14 [125].

4.2.2.2 Trilayered bioprinted scaffolds

In 2019, Nowicki et al. developed a continuous gradient 3D-printed osteochondral construct by combining several innovative bioinks to more accurately mimic the complex structure and properties of natural osteochondral tissue. A new approach was taken to develop an osteochondral matrix material using a PCL primary bioink and involved a bioink composed of polycaprolactone-triol, castor oil, and poly(hexamethylene diisocyanate). In addition, nano hydroxyapatite (nHAp) was synthesized and 3D-printed into subchondral bone layers, thereby improving its mechanical strength and helping the constructs realize favorable shape memory behavior. Furthermore, chondrogenic growth factors were introduced into the cartilage layer. The resulting PCL+bovine serum albumin (BSA)/TGF-β1 construct significantly outperformed other combinations with respect to total collagen and type 2 collagen synthesis, both of which are crucial for chondrogenesis. Taken together, these findings suggest promising new directions for investigations into cartilaginous and osteochondral responses within the field of tissue engineering [126].

In 2020, Kilian et al. proposed a multi-layered bioprinted scaffold for the regeneration of full-thickness osteochondral defects. The associated bioinks were formulated using alginate methylcellulose (algMC) and HAp-forming calcium phosphate cement. The bioink of the first layer was formulated with algMC and 5×10^6 human chondrocytes per gram of the material and was crosslinked with $CaCl_2$ for 10 min. The second layer was printed by interweaving the cell-laden algMC bioink and calcium phosphate cement (without cells) via multi-channel extrusion-based printing; this was designed to mimic the formation of calcified cartilage. The third layer was printed using only calcium phosphate cement to mimic subchondral bone. Subsequent in vitro studies revealed that constructs were able to support cell growth and the deposition of essential ECM molecules. Further studies should be conducted to explore different cell types that can be supported [127].

In 2021, Liu et al. developed a trilayered bioprinted scaffold to treat osteochondral defects in a rat model, as shown in Fig. 8d. In these scaffolds, the top-most anti-inflammatory layer was printed using diclofenac sodium (DC)-incorporated MMP-sensitive peptide-modified methacrylated hyaluronic acid (MeHA). The next layer was printed via multi-channel extrusion to assist in cartilage regeneration. The authors used two bioinks, bone marrow stem cell (BMSC)-loaded/MeHA and kartogenin-loaded polycaprolactone (KGN/PCL). The final layer was printed with β-TCP/PCL to regenerate subchondral bone. Chondrogenic differentiation of BMSCs has been reported by earlier in vitro studies and is thought to occur via the expression of aggrecan, Sox9, TGF-β1, and collagen type 2. Furthermore, MMP13 expression was reduced threefold after five days of culturing. Upon in vivo testing in a rat model, protein expression was quantified by the optical density of samples stained for immunohistochemical analysis. The authors found that IL-1β levels were significantly lower, whereas collagen type 2 was highly expressed at 12 weeks post-operation. Osteophyte formation and cartilage degeneration were also much lower in the treatment group than in the control group [128].

Finally, Singh et al. bioprinted an osteochondral model to mimic inflamed human joints. To do so, they used two bioinks, cartilage ink (SF-polyvinylpyrrolidone (PVP)) and bone ink (SF-PVP with nHAp) [129]. In these scaffolds, the calcified layer was replicated via both the cartilage and bone inks. The resulting morphology revealed an open porous structure with an estimated porosity of 80%–85% for composite constructs. These scaffolds were then found to induce specific proinflammatory molecules within the structure of the printed scaffold. Next, the authors tested treatments with anti-inflammatory drugs such as celecoxib (CXB) and rhein (RHN) and tracked specific markers of osteoarthritis, including structural degeneration. After drug treatment, the levels of inflammatory molecules such as NO and PGE2 decreased. Moreover, ADAMTS4 levels decreased significantly following CXB and RHN treatment. Anabolic markers (i.e., COL II, aggrecan, and OCN) were found to increase in healthy constructs and decrease following cytokine induction. Next, IL-6 levels increased significantly with increasing cytokine levels and increased further under increasing drug treatments. In addition, the expression of markers associated with cartilage breakdown (i.e., MMPs and aggrecanase-1) was found to be reduced [129]. While this study was performed to generate an inflammation-associated model for osteoarthritis, the scaffold design concept may also be applied for treating osteochondral defects.

4.2.3 Comparisons of bioprinting strategies for osteoarthritis treatment

Bioink-based methods use cell-encapsulated biomaterials for bioprinting 3D structures capable of mimicking tissue microarchitecture. Natural biomaterials such as collagen, alginate, hyaluronic acid, and gelatin are commonly used, since they are highly suitable for cartilage regeneration. The use of dECM-based materials has also become widespread. Scaffolding-based methods depend on the use of a synthetic biomaterial to construct an external, 3D-printed scaffold within which a hydrogel containing cells is housed. In general, scaffolds fabricated exclusively with bioinks reported mechanical strength values in the kPa range, whereas those fabricated using scaffolding-based methods have superior mechanical strength, usually in the MPa range. This difference can be attributed to the load-bearing function being assigned to 3D-printed scaffolds composed of synthetic biomaterials such as PCL and PU. Unlike bioink-based constructs, scaffolding-based constructs performed better in terms of degradability and shape retention post-implantation. Construct degradability is an important factor to consider, since cartilage regeneration can take anywhere between 6 and 18 months in humans [130]. One aspect that can be explored is a strategy to ensure effective crosslinking between the 3D-printed scaffold and the hydrogel, which can further improve construct stability.

While bioink- and scaffolding-based methods are both suitable for treating early-stage osteoarthritis, different strategies should be employed for targeting full-depth defects characteristic of Grade 3 and 4 osteoarthritis. Scaffolds with varying gradients and layers must therefore be designed to cater to the microarchitecture of the different zones present in articular cartilage. In a bilayered scaffold, the main strategy is to regenerate cartilage tissue and underlying subchondral bone separately. Trilayered scaffolds are also important for individually regenerating the calcified zone, which is mainly composed of hypertrophic chondrocytes, collagen type 1, and nHAp. In both strategies, more emphasis is given to ensuring proper zonal design and integration such that a full-depth defect can be regenerated entirely. Furthermore, scaffolds fabricated using both approaches had superior mechanical strength relative to methods that used bioink-based or scaffolding-based methods alone. Designs for cartilage layers included rectilinear and grid patterns, while designs for bone layers included more complex patterns such as honeycomb. Various drugs and bioactive factors like kartogenin, growth factors, and nonsteroidal anti-inflammatory drugs (NSAIDs) have also been successfully incorporated into bilayered and trilayered bioprinted scaffolds. The further addition of bioceramics such as nHAp and β-TCP along with synthetic polymers like PCL during the fabrication of calcified cartilage and subchondral bone zones was also found to aid in the regeneration of osseous tissue. Another aspect that can be explored is the introduction of unique designs for a tidemark layer when fabricating bioprinted scaffolds, as this approach remains underexplored [17]. Furthermore, advanced technologies such as volumetric bioprinting should be further developed to achieve high-resolution prints of complex geometries.

5 Conclusions

Significant progress has been made in the development of tissue-engineered products to treat osteoarthritis, but many of these products are still lacking in certain areas. For example, while viscosupplementation with products such as Atelocollagen® and EUFLEXXA® can provide pain relief, they need to be administered periodically and are therefore unfeasible long-term treatment options. Moreover, although they provide much-needed lubrication, they are ineffective in treating full-depth defects. In contrast, acellular implantable scaffolds such as ChonDux™ and TruFit® are mechanically stable and are designed to target cartilage and bone defects, while cellular scaffolds such as NeoCart® and BST-CarGel® have been found to successfully regenerate cartilage tissue. However, over the long run important limitations such as fibrosis and osteophyte formation persist. This could be because implantable scaffolds are heavily dependent on surgical procedures such as microfracture and arthrotomy. This exposes encapsulated chondrocytes and other cell types to the bone marrow microenvironment, ultimately resulting in the dedifferentiation of cells toward fibrocartilage formation. Furthermore, patients must be prescribed various drugs to combat the inflammation and antigenicity that result from these procedures. However, the use of exclusively natural biomaterials in scaffold fabrication can lead to issues with long-term stability. For example, collagen-based scaffolds often suffer from inadequate mechanical strength, thereby compromising their ability to withstand joint stress over time [131]. Similarly, while hyaluronic acid offers excellent biocompatibility and water retention, it is too unstable for prolonged mechanical function, which is critical in load-bearing applications for osteoarthritis treatment [132]. The next generation of tissue-engineered products for osteoarthritis treatment involves the adoption of novel strategies, such as the use of bioprinting to create custom scaffolds. In addition, the use of drugs or growth factors may be critical. Overall, bioprinting has advantages over other tissue engineering techniques, since it is a high-throughput method with the ability to recreate complex 3D tissue anatomy very precisely. Hybrid approaches that combine bioprinting with electrospinning or freeze-drying may enhance scaffold porosity and mechanical resilience in the future. Furthermore, various studies

have been carried out both in vitro and in vivo to test the suitability of a wide range of biomaterials, cell types, drugs, growth factors, and small molecules. These studies have successfully reported the regeneration of chondral and osteochondral defects; however, further in-depth research is still needed to confirm their use prior to clinical trials.

Advancements in scaffold fabrication for osteoarthritis treatment are needed to overcome current bioprinting limitations. Emerging techniques—such as self-assembling scaffolds using biomimetic materials—offer the potential to autonomously organize into complex structures, thereby improving tissue integration and reducing the need for surgical intervention [133, 134]. These materials are often known as smart biomaterials, and constitute the foundation of 4D printing and real-time in situ 3D printing technologies [133]. Smart biomaterials are also becoming easier to integrate within tissues, since they are now capable of responding to biological cues such as inflammation or mechanical stress by releasing growth factors or anti-inflammatory agents. These "smart scaffolds" can support tissue repair, minimize fibrosis, and dynamically regulate the immune response. The convergence of bioprinting, smart materials, and personalized medicine offers a promising future for osteoarthritis treatments, enabling tailored, adaptive therapies. Real-time in situ printing, in particular, could facilitate customized scaffold deployment directly at the injury site [133, 134]. Moreover, patient-specific scaffolds, crafted from imaging data, would better match the anatomy, facilitating enhanced integration and effectiveness. This can be achieved via 5D printing, which can deposit curved layers in all three axes along two rotational axes [134]. In addition, targeted drug delivery systems embedded within the smart scaffolds could release therapeutic agents directly at the site, thereby minimizing systemic side effects and improving clinical outcomes. In essence, future scaffold fabrication may revolutionize osteoarthritis treatment by becoming more responsive, precise, and personalized, three major goals of advanced regenerative medicine.

Supplementary Information The online version contains supplementary material available at https://doi.org/10.1631/bdm.2400363.

Acknowledgements The authors would like to thank the Department of Biotechnology (BT/PR50614/MED/32/984/2023), Manipal Research Board (MRB), Dr. TMA Pai Scholarship, and Manipal School of Life Sciences, Manipal Academy of Higher Education for providing all the facilities and support. Figures 4, 5, 7, and 8 were created using BioRender.com.

Author contributions PM: conceptualization, literature review, data analysis & interpretation, writing—original draft, and review & editing; VMB: data analysis & interpretation, writing—original draft, and review & editing; AKS: writing—review & editing and supervision; VP: writing—review & editing and supervision; MKP: writing—review & editing and supervision; KPG: writing—review & editing and supervision; BNS: conceptualization, writing—review & editing, and supervision.

Funding Open access funding provided by Manipal Academy of Higher Education, Manipal.

Declarations

Conflict of interest The authors declare that they have no conflict of interest.

Ethical approval This article does not contain any studies with human or animal subjects performed by any of the authors.

References

1. Sophia Fox AJ, Bedi A, Rodeo SA (2009) The basic science of articular cartilage: structure, composition, and function. Sports Health 1(6):461–468. https://doi.org/10.1177/1941738109350438
2. Eschweiler J, Horn N, Rath B et al (2021) The biomechanics of cartilage—an overview. Life 11(4):302. https://doi.org/10.3390/life11040302
3. Petitjean N, Canadas P, Royer P et al (2023) Cartilage biomechanics: from the basic facts to the challenges of tissue engineering. J Biomed Mater Res Part A 111(7):1067–1089. https://doi.org/10.1002/jbm.a.37478
4. Wuelling M, Vortkamp A (2011) Chondrocyte proliferation and differentiation. In: Camacho-Hübner C, Nilsson O, Sävendahl L (Eds.), Cartilage and Bone Development and Its Disorders. Karger, Switzerland, p.1–11. https://doi.org/10.1159/000328081
5. Chijimatsu R, Saito T (2019) Mechanisms of synovial joint and articular cartilage development. Cell Mol Life Sci 76(20):3939–3952. https://doi.org/10.1007/s00018-019-03191-5
6. Xia Y, Momot KI, Chen Z et al (2016) Introduction to cartilage. In: Xia Y, Momot K (Eds.), Biophysics and Biochemistry of Cartilage by NMR and MRI (1st Ed.). The Royal Society of Chemistry, p.1–43. https://doi.org/10.1039/9781782623663-00001
7. Yelin E, Weinstein S, King T (2016) The burden of musculoskeletal diseases in the United States. Semin Arthritis Rheum 46(3):259–260. https://doi.org/10.1016/j.semarthrit.2016.07.013
8. March L, Cross M, Lo C et al (2016) Osteoarthritis: a Serious Disease: Submitted to the U.S. Food and Drug Administration, p.1–103. https://www.oarsi.org/sites/default/files/docs/2016/oarsi_white_paper_oa_serious_disease_121416_1. pdf [Accessed on 25

February 2024]
9. Long HB, Liu Q, Yin HY et al (2022) Prevalence trends of site-specific osteoarthritis from 1990 to 2019: findings from the global burden of disease study 2019. Arthritis Rheumatol 74(7): 1172–1183. https://doi.org/10.1002/art.42089
10. Mishra P, Singh BN (2023) Tissue reconstructive and regenerative medicine approach as an anti-aging intervention: relevance to age-induced osteoarthritis. In: Rizvi SI (Ed.), Emerging Anti-Aging Strategies (1st Ed.). Springer Nature, Singapore, p.311–329. https://doi.org/10.1007/978-981-19-7443-4_17
11. McAlindon TE, LaValley MP, Gulin JP et al (2000) Glucosamine and chondroitin for treatment of osteoarthritis: a systematic quality assessment and meta-analysis. JAMA 283(11): 1469–1475. https://doi.org/10.1001/jama.283.11.1469
12. Guermazi A, Hunter DJ, Kloppenburg M (2023) Debate: intra-articular steroid injections for osteoarthritis–harmful or helpful? Osteoarthr Imag 3(3):100163. https://doi.org/10.1016/j.ostima.2023.100163
13. Loeser RF, Collins JA, Diekman BO (2016) Ageing and the pathogenesis of osteoarthritis. Nat Rev Rheumatol 12(7):412–420. https://doi.org/10.1038/nrrheum.2016.65
14. Gannon FH, Sokoloff L (1999) Histomorphometry of the aging human patella: histologic criteria and controls. Osteoarthr Cartil 7(2):173–181. https://doi.org/10.1053/joca.1998.0206
15. Lyons TJ, Stoddart RW, McClure SF et al (2005) The tidemark of the chondro-osseous junction of the normal human knee joint. J Mol Histol 36(3):207–215. https://doi.org/10.1007/s10735-005-3283-x
16. Wang WY, Ye RX, Xie WQ et al (2022) Roles of the calcified cartilage layer and its tissue engineering reconstruction in osteoarthritis treatment. Front Bioeng Biotechnol 10:911281. https://doi.org/10.3389/fbioe.2022.911281
17. Yildirim N, Amanzhanova A, Kulzhanova G et al (2023) Osteochondral interface: regenerative engineering and challenges. ACS Biomater Sci Eng 9(3):1205–1223. https://doi.org/10.1021/acsbiomaterials.2c01321
18. Chow YY, Chin KY (2020) The role of inflammation in the pathogenesis of osteoarthritis. Mediat Inflamm 2020(1):8293921. https://doi.org/10.1155/2020/8293921
19. Goldring MB, Otero M (2011) Inflammation in osteoarthritis. Curr Opin Rheumatol 23(5):471–478. https://doi.org/10.1097/bor.0b013e328349c2b1
20. Li MZ, Yin H, Yan ZN et al (2022) The immune microenvironment in cartilage injury and repair. Acta Biomater 140:23–42. https://doi.org/10.1016/j.actbio.2021.12.006
21. Saito T, Tanaka S (2017) Molecular mechanisms underlying osteoarthritis development: Notch and NF-κB. Arthritis Res Ther 19(1):94. https://doi.org/10.1186/s13075-017-1296-y
22. Suri S, Gill SE, de Camin SM et al (2007) Neurovascular invasion at the osteochondral junction and in osteophytes in osteoarthritis. Ann Rheum Dis 66(11):1423–1428. https://doi.org/10.1136/ard.2006.063354
23. Erggelet C, Vavken P (2016) Microfracture for the treatment of cartilage defects in the knee joint–a golden standard? J Clin Orthop Trauma 7(3):145–152. https://doi.org/10.1016/j.jcot.2016.06.015
24. Izadifar Z, Chen XB, Kulyk W (2012) Strategic design and fabrication of engineered scaffolds for articular cartilage repair. J Funct Biomater 3(4):799–838. https://doi.org/10.3390/jfb3040799
25. Davies RL, Kuiper NJ (2019) Regenerative medicine: a review of the evolution of autologous chondrocyte implantation (ACI) therapy. Bioengineering 6(1):22. https://doi.org/10.3390/bioengineering6010022
26. Thorp H, Kim K, Kondo M et al (2021) Trends in articular cartilage tissue engineering: 3d mesenchymal stem cell sheets as candidates for engineered hyaline-like cartilage. Cells 10(3):643. https://doi.org/10.3390/cells10030643
27. Pritzker KPH, Gay S, Jimenez SA et al (2006) Osteoarthritis cartilage histopathology: grading and staging. Osteoarthr Cartil 14(1):13–29. https://doi.org/10.1016/j.joca.2005.07.014
28. Prezja F, Annala L, Kiiskinen S et al (2024) Exploring the efficacy of base data augmentation methods in deep learning-based radiograph classification of knee joint osteoarthritis. Algorithms 17(1):8. https://doi.org/10.3390/a17010008
29. Ebata T, Terkawi MA, Hamasaki M et al (2021) Flightless I is a catabolic factor of chondrocytes that promotes hypertrophy and cartilage degeneration in osteoarthritis. iScience 24(6):102643. https://doi.org/10.1016/j.isci.2021.102643
30. Sengprasert P, Kamenkit O, Tanavalee A et al (2024) The immunological facets of chondrocytes in osteoarthritis: a narrative review. J Rheumatol 51(1):13–24. https://doi.org/10.3899/jrheum.2023-0816
31. Silva JC, Carvalho MS, Han XR et al (2019) Compositional and structural analysis of glycosaminoglycans in cell-derived extracellular matrices. Glycoconj J 36(2):141–154. https://doi.org/10.1007/s10719-019-09858-2
32. Erisken C, Kalyon DM, Wang HJ (2008) Functionally graded electrospun polycaprolactone and beta-tricalcium phosphate nanocomposites for tissue engineering applications. Biomaterials 29(30):4065–4073. https://doi.org/10.1016/j.biomaterials.2008.06.022
33. Erisken C, Kalyon DM, Wang HJ et al (2011) Osteochondral tissue formation through adipose-derived stromal cell differentiation on biomimetic polycaprolactone nanofibrous scaffolds with graded insulin and beta-glycerophosphate concentrations. Tissue Eng Part A 17(9/10):1239–1252. https://doi.org/10.1089/ten.TEA.2009.0693
34. Zhao FH, Xiong Y, Ito K et al (2021) Porous geometry guided micro-mechanical environment within scaffolds for cell mechanobiology study in bone tissue engineering. Front Bioeng Biotechnol 9:736489. https://doi.org/10.3389/fbioe.2021.736489
35. Gupta D, Singh AK, Kar N et al (2019) Modelling and optimization of NaOH-etched 3-D printed PCL for enhanced cellular attachment and growth with minimal loss of mechanical strength. Mater Sci Eng C 98:602–611. https://doi.org/10.1016/j.msec.2018.12.084
36. Li JH, Ding MM, Fu Q et al (2008) A novel strategy to graft RGD peptide on biomaterials surfaces for endothelization of small-diamater vascular grafts and tissue engineering blood vessel. J Mater Sci Mater Med 19(7):2595–2603. https://doi.org/10.1007/s10856-007-3354-5
37. Kondyurin A, Lau K, Tang FY et al (2018) Plasma ion implantation of silk biomaterials enabling direct covalent immobilization of bioactive agents for enhanced cellular responses. ACS Appl Mater Interfaces 10(21):17605–17616. https://doi.org/10.1021/acsami.8b03182
38. Heller GZ, Manuguerra M, Chow R (2016) How to analyze the visual analogue scale: myths, truths and clinical relevance. Scand J Pain 13:67–75. https://doi.org/10.1016/j.sjpain.2016.06.012
39. Gandek B (2015) Measurement properties of the Western Ontario

and McMaster Universities Osteoarthritis Index: a systematic review. Arthritis Care Res 67(2):216–229. https://doi.org/10.1002/acr.22415
40. Pham T, van der Heijde D, Altman RD et al (2004) OMERACT-OARSI Initiative: Osteoarthritis Research Society International set of responder criteria for osteoarthritis clinical trials revisited. Osteoarthr Cartil 12(5):389–399. https://doi.org/10.1016/j.joca.2004.02.001
41. Higgins LD, Taylor MK, Park D et al (2007) Reliability and validity of the International Knee Documentation Committee (IKDC) subjective knee form. Joint Bone Spine 74(6):594–599. https://doi.org/10.1016/j.jbspin.2007.01.036
42. Paatela T, Vasara A, Nurmi H et al (2020) Assessment of cartilage repair quality with the International Cartilage Repair Society score and the Oswestry Arthroscopy score. J Orthop Res 38(3):555–562. https://doi.org/10.1002/jor.24490
43. Yin SM, Njai R, Barker L et al (2016) Summarizing health-related quality of life (HRQOL): development and testing of a one-factor model. Popul Health Metr 14:22. https://doi.org/10.1186/s12963-016-0091-3
44. Devlin N, Parkin D, Janssen B (2020) An introduction to EQ-5D instruments and their applications. In: Devlin N, Parkin D, Janssen B (Eds.), Methods for Analysing and Reporting EQ-5D Data (1st Ed.). Springer, Cham, p.1–22. https://doi.org/10.1007/978-3-030-47622-9_1
45. Schreiner MM, Raudner M, Marlovits S et al (2021) The MOCART (magnetic resonance observation of cartilage repair tissue) 2.0 knee score and atlas. Cartilage 13:571S–587S. https://doi.org/10.1177/1947603519865308
46. Mamisch TC, Trattnig S, Quirbach S et al (2010) Quantitative T2 mapping of knee cartilage: differentiation of healthy control cartilage and cartilage repair tissue in the knee with unloading: initial results. Radiology 254(3):818–826. https://doi.org/10.1148/radiol.09090335
47. Briggs KK, Steadman JR, Hay CJ et al (2009) Lysholm score and Tegner activity level in individuals with normal knees. Am J Sports Med 37(5):898–901. https://doi.org/10.1177/0363546508330149
48. Collins NJ, Prinsen CAC, Christensen R et al (2016) Knee injury and osteoarthritis outcome score (KOOS): systematic review and meta-analysis of measurement properties. Osteoarthr Cartil 24(8):1317–1329. https://doi.org/10.1016/j.joca.2016.03.010
49. Lins L, Carvalho FM (2016) SF-36 total score as a single measure of health-related quality of life: scoping review. SAGE Open Med 4:2050312116671725. https://doi.org/10.1177/2050312116671725
50. Salthouse D, Novakovic K, Hilkens CMU et al (2023) Interplay between biomaterials and the immune system: challenges and opportunities in regenerative medicine. Acta Biomater 155: 1–18. https://doi.org/10.1016/j.actbio.2022.11.003
51. Tripathi AS, Zaki MEA, Al-Hussain SA et al (2023) Material matters: exploring the interplay between natural biomaterials and host immune system. Front Immunol 14:1269960. https://doi.org/10.3389/fimmu.2023.1269960
52. Cohen MC (1982) Characterization of the lymphokine responsible for migration-inhibitory activity against tumor cells. Cancer Res 42(6):2135–2138.
53. Nees TA, Rosshirt N, Zhang JA et al (2019) Synovial cytokines significantly correlate with osteoarthritis-related knee pain and disability: inflammatory mediators of potential clinical relevance. J Clin Med 8(9):1343. https://doi.org/10.3390/jcm8091343
54. Nakashima M, Sakai T, Hiraiwa H et al (2012) Role of S100A12 in the pathogenesis of osteoarthritis. Biochem Biophys Res Commun 422(3):508–514. https://doi.org/10.1016/j.bbrc.2012.05.036
55. Bellamy N, Campbell J, Robinson V et al (2006) Viscosupplementation for the treatment of osteoarthritis of the knee. Cochrane Database Syst Rev 2006(2):CD005321. https://doi.org/10.1002/14651858.CD005321.pub2
56. Miyata T, Taira T (1990) Aqueous atelocollagen solution and method of preparing same. https://patents.google.com/patent/EP0132979B1/en [Accessed on 19 January 2024]
57. Suh DS, Yoo JC, Woo SH et al (2021) Intra-articular atelocollagen injection for the treatment of articular cartilage defects in rabbit model. Tissue Eng Regen Med 18(4):663–670. https://doi.org/10.1007/s13770-021-00337-0
58. Lee HS, Oh KJ, Moon YW et al (2021) Intra-articular injection of type I atelocollagen to alleviate knee pain: a double-blind, randomized controlled trial. Cartilage 13(1_suppl):342S–350S. https://doi.org/10.1177/1947603519865304
59. Smith MM, Russell AK, Schiavinato A et al (2013) A hexadecylamide derivative of hyaluronan (HYMOVIS®) has superior beneficial effects on human osteoarthritic chondrocytes and synoviocytes than unmodified hyaluronan. J Inflamm 10:26. https://doi.org/10.1186/1476-9255-10-26
60. Oliviero F, Scanu A, Frallonardo P et al (2012) AB0083 anti-inflammatory effect of Hymovis® on an in vitro model of CPP crystal-induced inflammation. Comparison with other hyaluronic acids used for intra-articular treatment. Ann Rheum Dis 71:642. https://doi.org/10.1136/annrheumdis-2012-eular.83
61. Benazzo F, Perticarini L, Padolino A et al (2016) A multicentre, open label, long-term follow-up study to evaluate the benefits of a new viscoelastic hydrogel (Hymovis®) in the treatment of knee osteoarthritis. Eur Rev Med Pharmacol Sci 20(5): 959–968
62. Nascimento LD, Nicoletti NF, Peletti-Figueiró M et al (2021) Hyaluronic acid in vitro response: viability and proliferation profile of human chondrocytes in 3D-based culture. Cartilage 13(2_suppl):1077S–1087S. https://doi.org/10.1177/19476035211057244
63. Chevalier X, Jerosch J, Goupille P et al (2010) Single, intra-articular treatment with 6 ml hylan G-F 20 in patients with symptomatic primary osteoarthritis of the knee: a randomised, multicentre, double-blind, placebo controlled trial. Ann Rheum Dis 69(1):113–119. https://doi.org/10.1136/ard.2008.094623
64. Altman RD, Rosen JE, Bloch DA et al (2009) A double-blind, randomized, saline-controlled study of the efficacy and safety of EUFLEXXA® for treatment of painful osteoarthritis of the knee, with an open-label safety extension (the FLEXX trial). Semin Arthritis Rheum 39(1):1–9. https://doi.org/10.1016/j.semarthrit.2009.04.001
65. Karperien M (2024) Technology-Hy2Care. https://www.hy2care.com/en/technology [Accessed on 13 April 2024]
66. Jin R, Teixeira LSM, Dijkstra PJ et al (2010) Enzymatically-crosslinked injectable hydrogels based on biomimetic dextran-hyaluronic acid conjugates for cartilage tissue engineering. Biomaterials 31(11):3103–3113. https://doi.org/10.1016/j.biomaterials.2010.01.013
67. Sharma B, Fermanian S, Gibson M et al (2013) Human cartilage repair with a photoreactive adhesive-hydrogel composite. Sci Transl Med 5(167):167ra6. https://doi.org/10.1126/scitranslmed.3004838
68. Wolf MT, Zhang H, Sharma B et al (2020) Two-year follow-up

and remodeling kinetics of ChonDux hydrogel for full-thickness cartilage defect repair in the knee. Cartilage 11(4):447–457. https://doi.org/10.1177/1947603518800547
69. D'Ambrosi R, Valli F, De Luca P et al (2019) MaioRegen osteochondral substitute for the treatment of knee defects: a systematic review of the literature. J Clin Med 8(6):783. https://doi.org/10.3390/jcm8060783
70. Kon E, Filardo G, Perdisa F et al (2014) Clinical results of multilayered biomaterials for osteochondral regeneration. J Exp Orthop 1(1):10. https://doi.org/10.1186/s40634-014-0010-0
71. Kon E, Delcogliano M, Filardo G et al (2011) Novel nanocomposite multilayered biomaterial for osteochondral regeneration: a pilot clinical trial. Am J Sports Med 39(6):1180–1190. https://doi.org/10.1177/0363546510392711
72. Perdisa F, Kon E, Sessa A et al (2018) Treatment of knee osteochondritis dissecans with a cell-free biomimetic osteochondral scaffold: clinical and imaging findings at midterm follow-up. Am J Sports Med 46(2):314–321. https://doi.org/10.1177/0363546517737763
73. Dell'Osso G, Bottai V, Bugelli G et al (2016) The biphasic bioresorbable scaffold (Trufit®) in the osteochondral knee lesions: long-term clinical and MRI assessment in 30 patients. Musculoskelet Surg 100(2):93–96. https://doi.org/10.1007/s12306-015-0383-y
74. Azam A, Forster M, Robertson A (2018) Clinical and radiological outcome for Trufit plug in the treatment of chondral and osteochondral lesions at a minimum of 2 years. J Orthop 15(1): 47–51. https://doi.org/10.1016/j.jor.2018.01.001
75. Shivji FS, Mumith A, Yasen S et al (2020) Treatment of focal chondral lesions in the knee using a synthetic scaffold plug: long-term clinical and radiological results. J Orthop 20:12–16. https://doi.org/10.1016/j.jor.2020.01.015
76. Harley BA, Lynn AK, Wissner-Gross Z et al (2010) Design of a multiphase osteochondral scaffold III: fabrication of layered scaffolds with continuous interfaces. J Biomed Mater Res A 92(3):1078–1093. https://doi.org/10.1002/jbm.a.32387
77. Berta A, Shive MS, Lynn AK et al (2020) Follow-up study evaluating the long term outcome of ChondroMimetic in the treatment of osteochondral defects in the knee. Appl Sci 10(16): 5642. https://doi.org/10.3390/app10165642
78. Iwasa J, Engebretsen L, Shima Y et al (2009) Clinical application of scaffolds for cartilage tissue engineering. Knee Surg Sports Traumatol Arthrosc 17(6):561–577. https://doi.org/10.1007/s00167-008-0663-2
79. Marcacci M, Berruto M, Brocchetta D et al (2005) Articular cartilage engineering with Hyalograft® C: 3-year clinical results. Clin Orthop Relat Res (435):96–105. https://doi.org/10.1097/01.blo.0000165737.87628.5b
80. Shive MS, Stanish WD, McCormack R et al (2015) BST-CarGel® treatment maintains cartilage repair superiority over microfracture at 5 years in a multicenter randomized controlled trial. Cartilage 6(2):62–72. https://doi.org/10.1177/1947603514562064
81. Stanish WD, McCormack R, Forriol F et al (2013) Novel scaffold-based BST-CarGel treatment results in superior cartilage repair compared with microfracture in a randomized controlled trial. J Bone Joint Surg Am 95(18):1640–1650. https://doi.org/10.2106/JBJS.L.01345
82. Park YB, Ha CW, Lee CH et al (2017) Cartilage regeneration in osteoarthritic patients by a composite of allogeneic umbilical cord blood-derived mesenchymal stem cells and hyaluronate hydrogel: results from a clinical trial for safety and proof-of-concept with 7 years of extended follow-up. Stem Cells Transl Med 6(2):613–621. https://doi.org/10.5966/sctm.2016-0157
83. Nehrer S, Halbwirth F, Luksch T (2014) CaReS®, cartilage regeneration system: autologous chondrocyte transplantation in a collagen gel. In: Shetty AA, Kim SJ, Nakamura N et al (Eds.), Techniques in Cartilage Repair Surgery (1st Ed.). Springer, Heidelberg, Germany, p.245–250. https://doi.org/10.1007/978-3-642-41921-8_21
84. Crawford DC, Heveran CM, Cannon WD et al (2009) An autologous cartilage tissue implant NeoCart for treatment of grade III chondral injury to the distal femur: prospective clinical safety trial at 2 years. Am J Sports Med 37(7):1334–1343. https://doi.org/10.1177/0363546509333011
85. Kane MS, Williams RJ, DeBerardino TM et al (2018) Review of an exploratory phase II FDA regulated clinical trial of a novel surgical innovation: completion of a prospective, randomized, controlled trial to compare NeoCart with the standard-of-care, microfracture, for articular cartilage repair. Ann Joint 3:69. https://doi.org/10.21037/aoj.2018.06.08
86. Clavé A, Potel JF, Servien E et al (2016) Third-generation autologous chondrocyte implantation versus mosaicplasty for knee cartilage injury: 2-year randomized trial. J Orthop Res 34(4): 658–665. https://doi.org/10.1002/jor.23152
87. Selmi TAS, Verdonk P, Chambat P et al (2008) Autologous chondrocyte implantation in a novel alginate-agarose hydrogel: outcome at two years. J Bone Joint Surg Br 90(5):597–604. https://doi.org/10.1302/0301-620X.90B5.20360
88. Wasyłeczko M, Sikorska W, Chwojnowski A (2020) Review of synthetic and hybrid scaffolds in cartilage tissue engineering. Membranes 10(11):348. https://doi.org/10.3390/membranes10110348
89. Lammi MJ, Piltti J, Prittinen J et al (2018) Challenges in fabrication of tissue-engineered cartilage with correct cellular colonization and extracellular matrix assembly. Int J Mol Sci 19(9): 2700. https://doi.org/10.3390/ijms19092700
90. Fuentes-Mera L, Camacho A, Moncada-Saucedo NK et al (2017) Current applications of mesenchymal stem cells for cartilage tissue engineering. In: van Pham P (Ed.), Mesenchymal Stem Cells - Isolation, Characterization and Applications (1st Ed.). InTech, p.149–184. https://doi.org/10.5772/intechopen.68172
91. Francis SL, Di Bella C, Wallace GG et al (2018) Cartilage tissue engineering using stem cells and bioprinting technology-barriers to clinical translation. Front Surg 5:70. https://doi.org/10.3389/fsurg.2018.00070
92. Bandyopadhyay A, Bose S, Das S (2015) 3D printing of biomaterials. MRS Bull 40(2):108–115. https://doi.org/10.1557/mrs.2015.3
93. Rider P, Kačarević ŽP, Alkildani S et al (2018) Bioprinting of tissue engineering scaffolds. J Tissue Eng 9:2041731418802090. https://doi.org/10.1177/2041731418802090
94. Cui XF, Boland T, D'Lima DD et al (2012) Thermal inkjet printing in tissue engineering and regenerative medicine. Recent Pat Drug Deliv Formul 6(2):149–155. https://doi.org/10.2174/187221112800672949
95. Li XD, Liu BX, Pei B et al (2020) Inkjet bioprinting of biomaterials. Chem Rev 120(19):10793–10833. https://doi.org/10.1021/acs.chemrev.0c00008
96. Wijshoff H (2010) The dynamics of the piezo inkjet printhead operation. Phys Rep 491(4–5):77–177. https://doi.org/10.1016/j.physrep.2010.03.003

97. Pati F, Jang J, Lee JW et al (2015) Extrusion bioprinting. In: Atala A, Yoo JJ (Eds.), Essentials of 3D Biofabrication and Translation (1st Ed.). Academic Press, USA, p.123–152. https://doi.org/10.1016/B978-0-12-800972-7.00007-4
98. Kumar H, Kim K (2020) Stereolithography 3D bioprinting. In: Crook JM (Ed.), 3D Bioprinting (1st Ed.). Humana, New York, USA, p.93–108. https://doi.org/10.1007/978-1-0716-0520-2_6
99. Raman R, Bashir R (2015) Stereolithographic 3D bioprinting for biomedical applications. In: Atala A, Yoo JJ (Eds.), Essentials of 3D Biofabrication and Translation (1st Ed.). Academic Press, USA, p.89–121. https://doi.org/10.1016/b978-0-12-800972-7.00006-2
100. Thomas G, Isaacs R (2011) Basic principles of lasers. Anaesth Intensive Care Med 12(12):574–577. https://doi.org/10.1016/j.mpaic.2011.09.013
101. Odde DJ, Renn MJ (2000) Laser-guided direct writing of living cells. Biotechnol Bioeng 67(3):312–318. https://doi.org/10.1002/(sici)1097-0290(20000205)67:3<312::aid-bit7>3.0.co;2-f
102. Dou CR, Perez V, Qu J et al (2021) A state-of-the-art review of laser-assisted bioprinting and its future research trends. ChemBioEng Rev 8(5):517–534. https://doi.org/10.1002/cben.202000037
103. Bernal PN, Bouwmeester M, Madrid-Wolff J et al (2022) Volumetric bioprinting of organoids and optically tuned hydrogels to build liver-like metabolic biofactories. Adv Mater 34(15): e2110054. https://doi.org/10.1002/adma.202110054
104. Bernal PN, Delrot P, Loterie D et al (2019) Volumetric bioprinting of complex living-tissue constructs within seconds. Adv Mater 31(42):e1904209. https://doi.org/10.1002/adma.201904209
105. Madrid-Wolff J, Toombs J, Rizzo R et al (2023) A review of materials used in tomographic volumetric additive manufacturing. MRS Commun 13(5):764–785. https://doi.org/10.1557/s43579-023-00447-x
106. Bernal PN, Delrot P, Loterie D et al (2019) Volumetric bioprinting of complex living-tissue constructs within seconds. Adv Mater 31(42):1904209. https://doi.org/10.1002/adma.201904209
107. Bhattacharjee T, Zehnder SM, Rowe KG et al (2015) Writing in the granular gel medium. Sci Adv 1(8): e1500655. https://doi.org/10.1126/sciadv.1500655
108. Highley CB, Rodell CB, Burdick JA (2015) Direct 3D printing of shear-thinning hydrogels into self-healing hydrogels. Adv Mater 27(34):5075–5079. https://doi.org/10.1002/adma.201501234
109. Hinton TJ, Jallerat Q, Palchesko RN et al (2015) Three-dimensional printing of complex biological structures by free-form reversible embedding of suspended hydrogels. Sci Adv 1(9):e1500758. https://doi.org/ 10.1126/sciadv.1500758
110. Shiwarski DJ, Hudson AR, Tashman JW et al (2021) Emergence of FRESH 3D printing as a platform for advanced tissue biofabrication. APL Bioeng 5(1):010904. https://doi.org/10.1063/5.0032777
111. Nguyen D, Hägg DA, Forsman A et al (2017) Cartilage tissue engineering by the 3D bioprinting of iPS cells in a nanocellulose/alginate bioink. Sci Rep 7(1):658. https://doi.org/10.1038/s41598-017-00690-y
112. Visscher DO, Lee H, van Zuijlen PPM et al (2021) A photo-crosslinkable cartilage-derived extracellular matrix bioink for auricular cartilage tissue engineering. Acta Biomater 121:193–203. https://doi.org/10.1016/j.actbio.2020.11.029
113. Gomes JM, Marques CF, Rodrigues LC et al (2024) 3D bioactive ionic liquid-based architectures: an anti-inflammatory approach for early-stage osteoarthritis. Acta Biomater 173: 298–313. https://doi.org/10.1016/j.actbio.2023.11.014
114. Galarraga JH, Kwon MY, Burdick JA (2019) 3D bioprinting via an in situ crosslinking technique towards engineering cartilage tissue. Sci Rep 9(1):19987. https://doi.org/10.1038/s41598-019-56117-3
115. Chen WM, Xu Y, Li YQ et al (2020) 3D printing electrospinning fiber-reinforced decellularized extracellular matrix for cartilage regeneration. Chem Eng J 382:122986. https://doi.org/10.1016/j.cej.2019.122986
116. Olmos-Juste R, Larrañaga-Jaurrieta G, Larraza I et al (2023) Alginate-waterborne polyurethane 3D bioprinted scaffolds for articular cartilage tissue engineering. Int J Biol Macromol 253: 127070. https://doi.org/10.1016/j.ijbiomac.2023.127070
117. Maihemuti A, Zhang H, Lin X et al (2023) 3D-printed fish gelatin scaffolds for cartilage tissue engineering. Bioact Mater 26: 77–87. https://doi.org/10.1016/j.bioactmat.2023.02.007
118. Wang H, Zhang JX, Liu H et al (2023) Chondrocyte-laden gelatin/sodium alginate hydrogel integrating 3D printed PU scaffold for auricular cartilage reconstruction. Int J Biol Macromol 253: 126294. https://doi.org/10.1016/j.ijbiomac.2023.126294
119. Sun Y, You YQ, Jiang WB et al (2020) 3D bioprinting dual-factor releasing and gradient-structured constructs ready to implant for anisotropic cartilage regeneration. Sci Adv 6(37): eaay1422. https://doi.org/10.1126/sciadv.aay1422
120. Wang SN, Luo B, Bai BS et al (2023) 3D printed chondrogenic functionalized PGS bioactive scaffold for cartilage regeneration. Adv Healthc Mater 12(27):e2301006. https://doi.org/10.1002/adhm.202301006
121. Nordberg RC, Huebner P, Schuchard KG et al (2021) The evaluation of a multiphasic 3D-bioplotted scaffold seeded with adipose derived stem cells to repair osteochondral defects in a porcine model. J Biomed Mater Res B Appl Biomater 109(12): 2246–2258. https://doi.org/10.1002/jbm.b.34886
122. Zhang X, Liu Y, Zuo Q et al (2021) 3D bioprinting of biomimetic bilayered scaffold consisting of decellularized extracellular matrix and silk fibroin for osteochondral repair. Int J Bioprint 7(4): 401. https://doi.org/10.18063/ijb.v7i4.401
123. Gu YQ, Zou YW, Huang YX et al (2023) 3D-printed biomimetic scaffolds with precisely controlled and tunable structures guide cell migration and promote regeneration of osteochondral defect. Biofabrication 16(1):015003. https://doi.org/10.1088/1758-5090/ad0071
124. Xu NJ, Lu DZ, Qiang L et al (2023) 3D-printed composite bioceramic scaffolds for bone and cartilage integrated regeneration. ACS Omega 8(41):37918–37926. https://doi.org/10.1021/acsomega.3c03284
125. Effanga VE, Akilbekova D, Mukasheva F et al (2024) In vitro investigation of 3D printed hydrogel scaffolds with electrospun tidemark component for modeling osteochondral interface. Gels 10(11):745. https://doi.org/10.3390/gels10110745
126. Nowicki M, Zhu W, Sarkar K et al (2020) 3D printing multiphasic osteochondral tissue constructs with nano to micro features via PCL based bioink. Bioprinting 17:e00066.

https://doi.org/10.1016/j.bprint.2019.e00066
127. Kilian D, Ahlfeld T, Akkineni AR et al (2020) 3D Bioprinting of osteochondral tissue substitutes-in vitro-chondrogenesis in multi-layered mineralized constructs. Sci Rep 10(1):8277. https://doi.org/10.1038/s41598-020-65050-9
128. Liu YZ, Peng LQ, Li LL et al (2021) 3D-bioprinted BMSC-laden biomimetic multiphasic scaffolds for efficient repair of osteochondral defects in an osteoarthritic rat model. Biomaterials 279:121216. https://doi.org/10.1016/j.biomaterials.2021.121216
129. Singh YP, Moses JC, Bandyopadhyay A et al (2022) 3D bioprinted silk-based in vitro osteochondral model for osteoarthritis therapeutics. Adv Healthc Mater 11(24):e2200209. https://doi.org/10.1002/adhm.202200209
130. Tuan RS, Chen AF, Klatt BA (2013) Cartilage regeneration. J Am Acad Orthop Surg 21(5):303–311. https://doi.org/10.5435/jaaos-21-05-303
131. Krych AJ, Harnly HW, Rodeo SA et al (2012) Activity levels are higher after osteochondral autograft transfer mosaicplasty than after microfracture for articular cartilage defects of the knee: a retrospective comparative study. J Bone Joint Surg Am 94(11):971–978. https://doi.org/10.2106/JBJS.K.00815
132. Collins MN, Birkinshaw C (2013) Hyaluronic acid based scaffolds for tissue engineering--a review. Carbohydr Polym 92(2): 1262–1279. https://doi.org/10.1016/j.carbpol.2012.10.028
133. Aldawood FK (2023) A comprehensive review of 4D printing: state of the arts, opportunities, and challenges. Actuators 12(3): 101. https://doi.org/10.3390/act12030101
134. Lai JH, Wang M (2023) Developments of additive manufacturing and 5D printing in tissue engineering. J Mater Res 38(21): 4692–4725. https://doi.org/10.1557/s43578-023-01193-5